HHS Public Access

Author manuscript

Neuroscience. Author manuscript; available in PMC 2022 January 01.

Published in final edited form as:

Neuroscience. 2021 January 01; 452: 247–264. doi:10.1016/j.neuroscience.2020.11.013.

Lmx1a and *Lmx1b* are redundantly required for the development of multiple components of the mammalian auditory system.

Victor V. Chizhikov[1,*], **Igor Y. Iskusnykh**[1], **Nikolai Fattakhov**[1], **Bernd Fritzsch**[2,*]

[1]Department of Anatomy and Neurobiology, The University of Tennessee Health Science Center, Memphis, TN 38163, USA

[2]Department of Biology, University of Iowa, Iowa, IA 52242, USA

Abstract

The inner ear, projections, and brainstem nuclei are essential components of the auditory and vestibular systems. It is believed that the evolution of complex systems depends on duplicated sets of genes. The contribution of duplicated genes to auditory or vestibular system development, however, is poorly understood. We describe that *Lmx1a* and *Lmx1b*, which originate from the invertebrate *Lmx1b*-like gene, redundantly regulate development of multiple essential components of the mammalian auditory/vestibular systems. Combined, but not individual, loss of *Lmx1a/b* eliminated the auditory inner ear organ of Corti and disrupted the spiral ganglion, which was preceded by a diminished expression of their critical regulator *Pax2*. Innervation of the remaining inner ear vestibular organs revealed unusual sizes or shapes and was more affected compared to *Lmx1a/b* single-gene mutants. Individual loss of *Lmx1a/b* genes did not disrupt brainstem auditory nuclei or inner ear central projections. Combined loss of *Lmx1a/b*, however, eliminated excitatory neurons in cochlear/vestibular nuclei, and also the expression of a master regulator *Atoh1* in their progenitors in the lower rhombic lip. Finally, in *Lmx1a/b* double mutants, vestibular afferents aberrantly projected to the roof plate. This phenotype was associated with altered expression of Wnt3a, a secreted ligand of the Wnt pathway that regulates pathfinding of inner ear projections. Thus, *Lmx1a/b* are redundantly required for the development of the mammalian inner ear, inner ear central projections, and cochlear/vestibular nuclei.

Keywords

LIM-homeodomain transcription factors; auditory system; neurosensory development; ear central projections; hindbrain; roof plate

[*]Corresponding authors: Victor V. Chizhikov, The University of Tennessee Health Science Center, Department of Anatomy and Neurobiology, vchizhik@uthsc.edu, phone: 1 (901) 448-2309, Bernd Fritzsch, University of Iowa, Department of Biology, bernd-fritzsch@uiowa.edu.

Author Contributions: VVC and BF conceptualized the work; BF performed dye labeling and immunohistochemistry experiments (Figures 1–3, 5–7) and analyzed data; VVC, IYI and NF performed immunohistochemistry and/or RNAscope *in situ* hybridization experiments (Figures 4, 8, 9) and analyzed data; BF wrote the original draft; VVC edited the paper.

Conflict of Interests: The authors declare no competing interests.

Introduction.

The vertebrate inner ear detects sounds and vestibular stimuli (Grothe et al., 2004; Fritzsch et al., 2013). Hair cells of the organ of Corti (OC) in the cochlea detect sounds that are transmitted by spiral ganglia neurons, which connect with brainstem cochlear nuclei (Macova et al., 2019; Filova et al., 2020). Vestibular components of the inner ear include anterior, horizontal and posterior canals cristae, which detect angular acceleration, and maculae in the utricle and saccule, which detect linear acceleration due to gravity, and connect via vestibular ganglia to the brainstem vestibular nuclei (Sienknecht et al., 2014; Fritzsch et al., 2019).

Transcription factors, including Pax2 and Atoh1, play an important role in auditory system development (Sanchez-Guardado *et al.* 2019). Loss of *Pax2* disrupts development of the cochlea (Bouchard *et al.* 2010). *Atoh1* is expressed in both the inner ear hair cells and the hindbrain lower rhombic lip (RL), which, gives rise to neurons of auditory and vestibular nuclei and some other excitatory neurons that populate the brainstem (Rose et al., 2009; Fujiyama et al., 2009). Loss of *Atoh1* prevents neuronal differentiation of RL progenitors and the development of hair cells in the inner ear, suggesting that *Atoh1* occupies a high position in the genetic network that regulates the development of the auditory system (Wang et al., 2005; Elliott et al., 2017).

It is believed that an origin and evolution of complex systems, such as the auditory and vestibular systems, critically depend on gene duplications. Genetic redundancy is essential to stabilize key developmental processes and allows one or both paralogs of duplicated genes to gradually change during evolution to accommodate the development of novel structures to support novel functions (Fritzsch and Elliott 2017). In vertebrates, LIM-homeodomain transcription factors Lmx1a and Lmx1b that arose from the invertebrate *Lmx1b*-like ancestral gene (Glover et al., 2018) have both unique and redundant functions. For example, *Lmx1b* has a unique function in the establishment of the isthmic organizer at the mid-hindbrain boundary, while *Lmx1a* has a non-redundant role in the regulation of the migration of granule progenitors from the cerebellar RL. In contrast, *Lmx1a/b* redundantly regulate differentiation of midbrain dopaminergic neurons (Doucet-Beaupré et al., 2015; Mishima et al., 2009; Chizhikov et al., 2010).

Lmx1a/b are also expressed in the inner ear in mouse and chicken (Huang et al., 2008; Mishima et al., 2009; Abello et al., 2010). In the mouse, *Lmx1a* is initially expressed throughout the otocyst, but, by embryonic day (e) 10.5, becomes restricted to non-sensory epithelia, where its expression continues at least up to the time of birth (Huang et al., 2008; Nichols et al., 2008; Koo et al., 2009). Although inner ear sensory epithelia cells do not express *Lmx1a*, short-term fate mapping confirmed that at least some of them originated from *Lmx1a*-expressing cells (Mann et al., 2017). qRT-PCR analysis revealed that in postnatal mice, some spiral ganglion neurons express *Lmx1a* (Grandi et al., 2020), although *in situ* hybridization did not find an expression of this gene in otic ganglia in mouse embryos (Huang et al., 2008). Analysis of *Lmx1a*−/− (*dreher*) mice revealed that in the inner ear, *Lmx1a* promotes cell commitment to non-sensory fate and regulates boundary formation between sensory and non-sensory epithelia. Loss of *Lmx1a* also leads to an ectopic

production of vestibular hair cells within the auditory sensory epithelium (Nichols et al., 2008; Koo et al., 2009; Mann et al., 2017; Huang et al. 2018; Nichols et al. 2020). Mutations in *LMX1A* have been described in patients with hearing deficits (Schrauwen et al. 2018; Wesdorp et al. 2018; Lee et al., 2020). In contrast to *Lmx1a*, in mouse embryos, weak expression of *Lmx1b* was reported in the inner ear sensory epithelium, mainly in hair cells, and in the cochleovestibular ganglion and spiral ganglion neurons (Huang et al., 2008). The function of *Lmx1b* in ear development has not been analyzed beyond experimental manipulations in chicken, which confirmed that chicken *Lmx1b* (*cLmx1b*) regulates expression of *Sox2, Bmp4,* and *Jag1.* Because cLmx1b is the functional homologue of mouse Lmx1a in the chicken inner ear (Mann et al., 2017; Huang et al. 2018), it remains unknown whether mouse *Lmx1b* regulates inner ear development alone or in interaction with *Lmx1a*.

In addition to expression in the inner ear, in the mouse hindbrain, *Lmx1a/b* are co-expressed in the roof plate, the dorsal-most cellular population, which produces secreted molecules regulating the specification of adjacent neuronal populations and axon guidance in the spinal cord and cerebellum (Millen et al., 2004; Chizhikov et al., 2006; Kridsada et al., 2018). Simultaneous, but not individual loss of *Lmx1a/b* genes ablates the development of the hindbrain roof plate (Mishima et al., 2009), suggesting that function of *Lmx1a/b* in the roof plate may be required for proper development of dorsally located auditory/vestibular brainstem nuclei or inner ear projections.

Here we report that in contrast to *Lmx1a/b* single-gene mutants, combined inactivation of *Lmx1a/b* completely prevents inner ear auditory development, disrupting OC and spiral ganglia. While cochlear and vestibular nuclei and inner ear central projections were essentially normal in *Lmx1a/b* single-gene mutants, loss of cochlear/vestibular brainstem neurons, and inner ear vestibular projections that aberrantly target the roof plate were observed in *Lmx1a/b* double knockout mice. These data show, for the first time, that evolutionarily related *Lmx1a/b* genes are required for the development of multiple essential components of the mammalian auditory system – the peripheral auditory neurosensory epithelium, central projections of the ears, and auditory and vestibular brainstem nuclei.

Materials and Methods.

Mice.

In this study we used *Lmx1a* null (*Lmx1a*^{drJ}, Jackson Laboratory strain #000636), (Millonig et al., 2000; Chizhikov et al., 2006) and *Lmx1b* null (Chen et al., 1998) mouse alleles. *Lmx1a* and *Lmx1b* knockout mice are referred to as *Lmx1a* KO and *Lmx1b* KO mice throughout this paper. To generate *Lmx1a* KO, *Lmx1b* KO and *Lmx1a/b* double knockout (DKO) embryos, *Lmx1a* and *Lmx1b* double heterozygous mice were crossed and embryos were collected at indicated stages. Noon of the day when a vaginal plug was observed was considered embryonic day 0.5 (e0.5). Mice were genotyped as previously described (Mishima et al., 2009). All live mouse work was approved by the University of Tennessee Health Science Center IACUC committee.

Lipophilic dye tracing.

Whole embryos at e11.5–12.5 or embryonic heads (for embryos older than e12.5) were fixed in 4% paraformaldehyde (PFA) in 0.1 M phosphate buffer with 300 mM sucrose (to minimize neuronal swelling) for 48 hrs. at 4°C and processed for dye tracing. To trace projections of the ear to the brain and of the brain to the ear we used NeuroVue dyes (NV Jade, NVJ; NV Red, NVR; NV Maroon, NVM) as previously described (Schmidt and Fritzsch, 2019). Lipophilic dyes were applied using dye-soaked filter strips, which provide a more precise and reliable way of a dye application compared to crystals or dye-injections (Schmidt and Fritzsch, 2019). In some cases, embryonic heads were split into two halves along the midline, and one half was used for dye tracing from the brain to the ear, while the other half – for tracing from the ear to the brain. To study the distribution of afferents relative to the brain dorsal midline, intact heads were used. Wavers soaked in different color dyes were appropriately shaped and inserted into the facial/inner ear efferent nerve root, into the rhombomere (r) 4 alar plate, and into the cerebellum to label inner ear efferents, spiral ganglion afferents, and vestibular afferents projecting to the cerebellum, respectively. For the tracing of inner ear central projections to the brain, the dye was placed into the otocyst to label the spiral ganglion, OC, and vestibular neurons. For the tracing of central projections of other cranial nerves to the brain, the dye was placed into their specific roots (Maklad et al., 2010). The dye was allowed to diffuse for 24–72 hrs. (depending on the type of dye and the age of the embryos) at 60°C in 4% PFA. Mutant and control embryos were always processed in parallel, with an identical dye placement and an identical dye diffusion time. Brains and ears were subsequently microdissected, mounted in glycerol and imaged using a Leica SP8 confocal microscope. After imaging, some brains and ears were post fixed in 4% PFA and either processed for immunohistochemistry (see below) or sectioned at 200 μm, mounted in glycerol, and imaged to reveal the distribution of projections in sections.

Immunohistochemistry.

Immunohistochemistry was performed using sections from either dye-labeling experiments (see above) or cryosections from embryos specifically prepared for immunohistochemistry as previously described (Mao et al. 2014; Iskusnykh et al. 2018). The following primary antibodies were used: mouse anti-Atoh1 (Developmental studies hybridoma bank, supernatant, 1:5), rabbit anti-Pax6 (Covance, Prb-278p-100, 1:300), rabbit anti-Tbr1 (Abcam, ab31490, 1:300), rabbit anti-Pax2 (Proteintech, 21385–1AP, 1:200), mouse anti-acetylated α-Tubulin (Sigma-Aldrich, T6793, 1:400), rabbit anti-Myosin 7 (Proteus, 25–6790,1:500), and rabbit anti-Neurofilament 200 (Sigma-Aldrich, N4142, 1:200). Appropriate secondary antibodies conjugated with Alexa 350, 488 or 594 fluorophores (Life Technologies) were used to detect primary antibodies. In some cases, Hoechst nuclear staining was used to visualize the tissue.

RNAscope *in situ* hybridization.

Embryos were fixed in 4% PFA in 0.1 M phosphate-buffered saline (PBS) for 16 hrs. at 4°C, sequentially cryoprotected in 10%, 20%, and 30% sucrose solutions in 0.1 M PBS, embedded in OCT, sagittally sectioned on a cryostat and mounted on Superfrost Plus slides (Fisher Scientific). All reagents were prepared using DEPC-treated water. RNAscope *in situ*

hybridization was performed using the RNAscope® 2.5 HD Reagent Kit-RED (Advanced Cell Diagnostics, Cat#322350) and a mouse *Wnt3a* RNAscope probe (20 ZZ pairs that recognize the target region 667 – 1634 of the mouse *Wnt3a* transcript NM_009522.2). The probe was designed and produced by Advanced Cell Diagnostics. *In situ* hybridization was performed according to the following protocol: slides were rinsed with PBS to remove OCT and dried for 2.5hrs. at room temperature. Then, sections were treated with H_2O_2 for 10 min., submerged in 1X Target retrieval solution (Cat#322000) for 5 min. at 98–100°C, rinsed in distilled water, dipped in 100% EtOH to remove excess water, and dried for 1h. Each section was treated with protease (Cat#322331) for 15 min. at 40°C and then rinsed in distilled water. Then, *Wnt3a* RNascope *in situ* hybridization probe was added to each section and incubated for 2 hrs. at 40°C. Unbound probe was removed by rinsing slides in 1X wash buffer (Cat#310091). Then, reagents for signal amplification (AMP1-AMP6, Cat#322311–14, Cat#322361–2) were sequentially added to each section according to the manufacturer's instructions. Finally, slides were washed twice in PBS and coverslipped with Fluoro-Gel mounting medium (Cat# 17985–10, Electron Microscopy Sciences).

Experimental design, image acquisition, and data analysis.

For each marker, at least three samples of each genotype at each developmental stage were analyzed. Both male and female embryos were used for analysis. Given the altered morphology of the *Lmx1ab* DKO brainstem, we identified cochlear nuclei based on Pax6 expression, as previously reported (Fujiyama et al., 2009). To ensure that we do not miss Pax6+ cochlear nuclei neurons, we generated series of transverse sections spanning the entire hindbrain and stained every section for Pax6 in control and *Lmx1a/b* mutants. During our analysis, we compared sections taken at the same anterior-posterior (A-P) levels of the hindbrain in control and *Lmx1a/b* mutant embryos. To facilitate the identification of the position of each section along the A-P axis, the same number of sections was placed on each slide. Fluorescent images were captured using a Zeiss Axio Imager A2 fluorescent Microscope equipped with a Zeiss AxioCam MRm camera and Axio Vision Rel 4.9 software (Zeiss) or a Leica SP8 confocal microscope. Mutant and control samples were co-imbedded, co-stained, and imaged under the same camera settings. Pax2 immunohistochemistry signal intensity in the inner ear of different genotypes and *Wnt3a* in situ hybridization signal intensity in the hindbrain roof plate of *Lmx1a/b* DKO embryos were determined using ImageJ (NIH) software. Pax2 quantification was performed in the left and right inner ears in three sections per embryo. Then, average Pax2 staining intensity was calculated for each embryo. *Wnt3a* staining intensity was determined using three sections from each A-P level per embryo. Statistical analysis of Pax2 intensity (comparison between multiple groups) was performed using one-way ANOVA with Tukey's post hoc test. Statistical analysis of *Wnt3a* intensity was performed using two-tailed t-test. Quantitative data are reported as mean ± standard deviation. $p<0.05$ was considered statistically significant. Picture panels were assembled using Adobe Photoshop or CorelDraw software.

Results

To identify whether *Lmx1a* and *Lmx1b* cooperate in the development of mammalian auditory and vestibular systems, we analyzed inner ears of *Lmx1a/b* single and double

mutants followed by the analysis of central projections of the ears and cochlear and vestibular brainstem nuclei.

Lack of inner ear auditory neurosensory development and aberrant inner ear vestibular innervation in *Lmx1a/b* double mutants.

To study the role of *Lmx1a/b* genes in inner ear development, we first analyzed inner ear innervation in *Lmx1a/b* single and double mutants at e12.5, when ear innervation begins (Nichols et al., 2008; Dvorakova et al., 2020). Similar to control (wild type) littermates (n=5 embryos), in e12.5 single-gene *Lmx1a* (*Lmx1a* KO) and *Lmx1b* (*Lmx1b* KO) mutants (n=3 embryos per genotype), anti-acetylated α-Tubulin immunostaining revealed the innervation of the auditory cochlear duct and vestibular anterior/horizontal and posterior canals cristae (Fig. 1A–C). While e12.5 *Lmx1a/b* double knockout (*Lmx1a/b* DKO) embryos showed an innervation toward the posterior canal crista, the innervation of the anterior/horizontal cristae was severely reduced, and an innervation of the cochlear duct was absent in all three *Lmx1a/b* DKO embryos investigated (Fig. 1D).

At e14.5, anti-acetylated α-Tubulin immunohistochemistry revealed an innervated OC in wild type, *Lmx1a* KO and *Lmx1b* KO embryos (n=3 embryos per genotype), while *Lmx1a/b* DKO littermates had only a cochlear sac-like extension without noticeable OC innervation (n=3/3 embryos) (Fig. 2A–D'). In contrast, innervation of all vestibular inner ear epithelia was recognizable in both single-gene and double e14.5 *Lmx1a/b* mutants (Fig. 2A"-D"'). Anterior/horizontal cristae fibers, however, appeared thinner in *Lmx1a/b* DKO mice (n=3/3 embryos) (Fig. 2A"-D"), while the innervation to posterior canal crista showed specific abnormalities in *Lmx1a* KO and *Lmx1a/b* DKO embryos (Fig. 2A"'-D"'). Compared to control littermates, in e14.5 *Lmx1a* KO embryos, posterior canal crista innervation was enlarged, consisting of multiple small branches, some of which aberrantly reached the basal turn of the cochlea (n=3/3 embryos) (Fig. 2A, B, A"', B"'). This unusual innervation likely reflects the previously reported partial transformation of OC into an irregular epithelium that shows a mix of vestibular and cochlear hair cells, resulting in the formation of an aberrant cochlear-vestibular organ (CVO) in addition to a caudally located OC (Nichols et al., 2008; Nichols et al., 2020). In *Lmx1a/b* DKO embryos, posterior canal crista innervation consisted of multiple large and small branches that ran across the otocyst (n=3/3 embryos) (Fig. 2A"', D"'), the phenotype that was also observed at earlier stages (Fig. 1D).

To test whether inner ear abnormalities in *Lmx1a/b* mutants were transient or resulted in permanent deficits, we compared *Lmx1a/b* mutants with wild type controls (n=4 embryos) at e18.5, when mature inner ear structure is largely achieved (Kersigo et al., 2011), and which is the last viable stage for *Lmx1a/b* DKO mice (Mishima et al., 2009). Specifically, labeling afferents and efferents with lipophilic dyes, identified spiral ganglia and showed a fully developed and innervated OC and only minor vestibular innervation abnormalities, including partially fused anterior and horizontal cristae fibers and reduced posterior crista fibers, in e18.5 *Lmx1b* KO (n=4/4) embryos (Fig. 3A, B). e18.5 *Lmx1a* KO mice showed partially fused anterior and horizontal cristae fibers, and fiber projections to the saccule fused with that to cochlea, containing aberrant CVO (Fig. 3C). Similar to earlier stages, in e18.5 *Lmx1a* KO embryos posterior canal crista innervation was enlarged and extensively branched

(n=4/4 embryos). As in control and *Lmx1b* KO embryos, spiral ganglia were consistently labeled in *Lmx1a* KO embryos (n=4/4) (Fig. 3C). In contrast, inner ears from all four investigated e18.5 *Lmx1a/b* DKO embryos revealed complete absence of OC and cochlear innervation and the lack of spiral ganglion labeling (Fig. 3D). Only a single bundle to the anterior/horizontal cristae was present. Innervation toward the utricle was reduced. As in younger embryos, innervation toward the posterior canal crista was enlarged and excessively branched (Fig. 3D).

To complement dye labeling, we also investigated inner ear innervation using immunohistochemistry against α-Tubulin, and sensory hair cells using immunohistochemistry against Myo7, a protein required for the development of hair bundles and proper functioning of hair cells (Boeda et al., 2002; Grati and Kachar, 2011; Kim et al., 2017). This analysis revealed that although vestibular sensory epithelia were still present in appropriate locations (anterior crista, utricle, saccule) in *Lmx1a/b* DKO embryos, no Myo7a labeling or α-Tubulin+ fibers were detected in the cochlear sac in any of three *Lmx1a/b* DKO embryos investigated (Fig. 3E–E"'), confirming the lack of OC development.

In conclusion, loss of *Lmx1a* and *Lmx1b* leads to specific inner ear abnormalities (Fig. 3G–J, Table 1). Loss of *Lmx1b* alone caused the least effect, resulting in only minimally affected vestibular innervation. Loss of *Lmx1a* alone leads to an intermediate effect with partially fused projections to saccule and cochlea, formation of an aberrant CVO, and other, more minor, vestibular innervation abnormalities. *Lmx1a/b* DKO mice showed the most severe phenotype with a complete lack of inner ear auditory development and innervation, and additional vestibular innervation abnormalities. The inner ear phenotype of *Lmx1a/b* DKO mice, especially lack of auditory development, exceeds summation of single-gene mutant phenotypes, indicating redundant function of *Lmx1a/b* during ear development.

Lmx1a and *Lmx1b* redundantly regulate expression of *Pax2*, a gene necessary for cochlear and spiral ganglion development.

Inner ears of *Lmx1a/b* DKO mice resemble those of *Pax2* mutant mice, which lack cochlear innervation, OC and spiral ganglia (Bouchard et al. 2010). To test whether *Lmx1a* and *Lmx1b* redundantly regulate inner ear development via *Pax2*, we studied *Pax2* expression in *Lmx1a/b* mutant mice. Based on immunohistochemistry, at e12, Pax2 is broadly expressed in the control inner ear, including the developing cochlear duct (Fig. 4A). In *Lmx1a/b* DKO but not *Lmx1a/b* single gene mutants, expression of *Pax2* was significantly ($p<0.05$) reduced in the ear (Fig. 4A–E), although this gene was still highly expressed in the adjacent hindbrain neural tube (Fig. 4D). Thus, *Lmx1a* and *Lmx1b* redundantly regulate expression of *Pax2* in the ear and likely regulate inner ear development, at least partially, via *Pax2*.

Simultaneous loss of *Lmx1a* and *Lmx1b* leads to an aberrant projection of inner ear afferents to the hindbrain roof plate.

Given the absence of auditory OC and spiral ganglia dye labeling in *Lmx1a/b* DKO mice, we focused on vestibular projections from the inner ear to the brainstem and compared them with adjacent cranial projection afferents. For this purpose, lipophilic dye was placed into the inner ear or roots of specific cranial nerves, and embryos were analyzed after the

appropriate time needed for dye diffusion. Inner ear afferents reach and enter the hindbrain in rhombomere 4 (r4) between e10 and e11. By e11.5 they extend anteriorly toward the cerebellum and posteriorly toward the obex parallel to the hindbrain roof plate in left and right halves of the brainstem, without entering or crossing the dorsal midline at this or later stages (Maklad et al., 2010). There was no obvious difference in central projections of the inner ear, trigeminal projections, or the solitary tract from cranial nerves VII, IX, X between wild type controls and *Lmx1a/b* single-gene mutants at e11.5 (n=3 embryos per genotype) (Fig. 5A–C'). In contrast, the inner ear central projections of *Lmx1a/b* DKO littermates deviated massively from those of control, *Lmx1a* KO and *Lmx1b* KO mice. Specifically, after entering the hindbrain, *Lmx1a/b* DKO inner ear afferents aberrantly projected to and crossed the dorsal midline roof plate, partially overlapping with trigeminal and solitary tract afferents (n=3/3 embryos) (Fig. 5D–H).

At e12.5, we were able to simultaneously label afferents from both ears. This analysis not only revealed that afferents from both left and right ears enter the roof plate in *Lmx1a/b* DKO embryos, but also that afferents from the opposite ears do not fuse, excluding each other (n=3/3 embryos) (Fig. 6A–C, E–G). The unusual projection of cranial nerves to the roof plate in *Lmx1a/b* DKO embryos, identified by the dye tracing, was also confirmed by immunohistochemistry in transverse sections, which revealed Neurofilament/acetylated α-Tubulin positive fibers extending across the roof plate in *Lmx1a/b* DKO but not control embryos (n=3 embryos per genotype) (Fig. 6D, H, I).

Notably, in *Lmx1a/b* DKO embryos, facial motor neurons and inner ear efferents (Fritzsch and Nichols 1993) showed normal bilateral location adjacent to the floor plate (n=3/3 embryos per stage) (Fig. 5E, F; 6E). Thus, while basal plate motor neuron development and connectivity was unaltered, the pathfinding of the inner ear, solitary tract and trigeminal fibers that normally target the alar plate, was specifically disrupted in *Lmx1a/b* DKO mice: rather than running parallel to the dorsal midline, these afferents abnormally project to and cross the undifferentiated roof plate in *Lmx1a/b* DKO mice.

Loss of *Lmx1a/b* disrupts anterior-posterior expansion of inner ear central projections.

Next, we studied the expansion of inner ear central projections and other cranial nerves along the anterior-posterior axis in more detail. Neurofilament antibody staining revealed the presence and appropriate location of all (V-XII) cranial nerve roots in e12.5 *Lmx1a/b* single and double mutant embryos (n=3 embryos per genotype) (Fig. 7A–H), indicating that overall anterior-posterior brainstem patterning was not grossly disrupted in any of these mutants.

Dye labeling revealed that while projections of cranial nerve IX were comparable between wild type controls and *Lmx1a/b* single and double mutants, anterior-posterior expansion of inner ear projections (nerve VIII) and trigeminal projections (nerve V) was altered in *Lmx1a/b* DKO (n=3/3) embryos. In particular, after entering the hindbrain in r4, inner ear projections (nerve VIII) did not extend posteriorly, while the trigeminal nerve (V) showed a massive expansion rostrally to the topographical equivalent of the cerebellum compared to control and single-gene *Lmx1a/b* mutants (Fig. 7I–P).

Combined, our data indicate that although general anterior-posterior hindbrain patterning is not dramatically affected in *Lmx1a/b* DKO embryos, simultaneous loss of *Lmx1a* and *Lmx1b* affects anterior-posterior expansion of inner ear central projections and trigeminal projections.

Simultaneous loss of *Lmx1a/b* alters expression of *Wnt3a* in the dorsal hindbrain.

Ear transplantation and gene knockout studies support the targeting of inner ear central projections to a dorsal source of secreted Wnt molecules in the hindbrain, at least partially via the Fzd3 Wnt receptor (Yang et al., 2017; Elliott and Fritzsch, 2018; Gordy et al., 2018; Duncan et al., 2019). Wnt3a activates both canonical and planar cell polarity Wnt signaling via several receptors, including Fzd3 (Endo et al., 2008; Rao and Kühl, 2010; Chang et al., 2014; Simonetti et al., 2014). In wild type embryos, *Wnt3a* is expressed in the lower RL, adjacent to the choroid plexus, along the anterior-posterior axis of the hindbrain (Parr et al., 1993; Hatch et al., 2007) (Fig. 8A). In *Lmx1a/b* DKO embryos, a smaller ectopic *Wnt3a* expression domain was observed in the roof plate (n=3/3 embryos), the region aberrantly populated by inner ear central projections in the double mutant mice (Fig. 8B). Consistent with a failed posterior expansion of inner ear central projections, virtually no *Wnt3a* expression (appeared just as a few dots in the roof plate) was detected in the posterior hindbrain of *Lmx1a/b* DKO mice (n=3/3 embryos) (Fig. 8C, D), suggesting that *Lmx1a/b* control pathfinding of inner ear central projections at least partially via regulating expression of secreted Wnt molecules.

Simultaneous loss of *Lmx1a* and *Lmx1b* compromises the development of cochlear and vestibular nuclei.

To study whether *Lmx1a* and *Lmx1b* are necessary for the development of cochlear and vestibular nuclei, we analyzed *Lmx1a/b* mutants at e18.5, when mature structure of these nuclei is largely achieved (Wang et al., 2005; Fujiyama et al., 2009). Previous studies identified *Pax6* as a specific marker of excitatory neurons in cochlear nuclei, while *Tbr1* marks excitatory neurons in the superior vestibular nuclei (Wang et al., 2005; Fujiyama et al., 2009). As in wild-type controls, numerous Pax6+ and Tbr1+ cells populated cochlear and superior vestibular nuclei, respectively, in *Lmx1a* KO and *Lmx1b* KO embryos (n=3 embryos per genotype) (Fig. 9A–D, F–I). In contrast, both Pax6+ and Tbr1+ neurons were absent in the corresponding nuclei in all three investigated e18.5 *Lmx1a/b* DKO mutants (Fig. 9E, J).

During development, excitatory neurons of both cochlear and vestibular nuclei originate from *Atoh1+* progenitors in the lower RL, a transient embryonic germinal zone that arises adjacent to the IVth ventricle roof plate (Wang et al., 2005; Rose et al., 2009; Nothwang, 2016). Atoh1 immunohistochemistry revealed neuronal progenitors in the lower RL of wild type and *Lmx1a and Lmx1b* single-gene mutants at e12 (n=3 embryos per genotype) (Fig. 9K, M–O'), when neurons are actively generated from *Atoh1+* RL progenitors (Wang et al., 2005; Rose et al., 2009). In contrast, no *Atoh1+* cells were detected in the lower RL in any of three comparably staged *Lmx1a/b* double mutants (Fig. 9L, P, P'), suggesting that the loss of excitatory cochlear and vestibular neurons that we observed in e18.5 *Lmx1a/b* DKO embryos results from lower RL progenitor defects at earlier stages.

Taken together, our data indicate that simultaneous, but not individual loss of *Lmx1a/b* prevents the formation of excitatory cochlear/vestibular nuclei neurons, revealing that similar to inner ear development and pathfinding of central projections, development of hindbrain auditory nuclei neurons redundantly require *Lmx1a* and *Lmx1b*.

Discussion.

The LIM-homeodomain transcription factors Lmx1a and Lmx1b represent a vertebrate duplication of the invertebrate *Lmx1b*-like gene (Glover et al., 2018) and have both unique and shared roles in the development of the mammalian cerebral cortex, midbrain dopaminergic neurons, cerebellum, and spinal cord interneurons (Doucet-Beaupré et al., 2015; Chizhikov et al., 2019). Here we report that combined, but not individual, loss of *Lmx1a/b* prevents auditory inner ear development, ablates excitatory neurons in the cochlear/vestibular nuclei, and disrupts pathfinding of the inner ear central projections (Fig. 10). Thus, this study, for the first time, shows that development of multiple components of the mammalian auditory and vestibular systems redundantly depend on *Lmx1a/b*.

Lmx1a and *Lmx1b* are redundantly required for the development of brainstem cochlear and vestibular nuclei.

Excitatory neurons of both cochlear and vestibular nuclei originate from *Atoh1*+ progenitors in the RL. The former arise from the lower RL in r2–5, while the latter arise from the RL extending from a posterior domain of r1 to r8 (Farago et al., 2006; Fujiyama et al., 2009; Di Bonito et al., 2017; Lipovsek and Wingate, 2018). Loss of *Atoh1* prevents the development of both cochlear and vestibular excitatory neurons, demonstrating that *Atoh1* is a master regulatory gene for these neurons (Wang et al., 2005; Elliott et al., 2017).

Here we show that loss of only one *Lmx1a/b* gene had no significant effect on the formation of cochlear or vestibular nuclei. In contrast, in *Lmx1a/b* DKO mice, both cochlear and vestibular nuclei were compromised, as revealed by the lack of expression of markers specific to their excitatory neurons and inner ear projections to alar plate regions normally occupied by these nuclei. *Lmx1a/b* DKO cochlear/vestibular nuclei abnormalities were preceded by the lack of *Atoh1* expression in the lower RL, suggesting that *Lmx1a/b* support cochlear/vestibular nuclei development by maintaining *Atoh1* expression in their progenitors.

In early r2–8, *Lmx1b* is expressed in the roof plate and in dA3/dB3 neurons, while *Lmx1a* is specifically expressed in the roof plate (Landsberg et al., 2005; Mishima et al. 2009; Sieber et al. 2009; Iskusnykh et al., 2016). Thus, the only r2–8 hindbrain region where *Lmx1a/b* are co-expressed in early (before e13) embryogenesis is the roof plate, the signaling center known to induce the upper RL (in r1) via secreted Bmp molecules (Chizhikov et al., 2006). Combined loss of *Lmx1a/b* disrupts hindbrain roof plate differentiation and signaling, resulting in a compromised cerebellum (Mishima et al., 2009), whose excitatory neurons originate from the upper RL (Machold and Fishell, 2005; Wang et al., 2005; Butts et al., 2014). Whether hindbrain roof plate regulates the development of the functionally distinct auditory lower RL was not specifically investigated. Our current study reporting loss of excitatory cochlear/vestibular neurons and *Atoh1* expression in the lower RL in *Lmx1a/b*

double mutants, however, strongly suggests that similar to the upper RL, *Lmx1a/b*-dependent roof plate also regulates the development of the lower RL and its neuronal progeny.

Both cochlear and vestibular nuclei contain not only excitatory but also inhibitory neurons, at least some of which originate from *Ptf1a*-expressing progenitors located ventral to the *Atoh1*+ RL (Fujiyama et al., 2009). Whether *Lmx1a/b* are essential for the development of inhibitory cochlear or vestibular nuclei neurons remains to be investigated.

It is important to note that in addition to neurons of cochlear/vestibular nuclei and cerebellar neurons, RL also gives rise to a broad array of other excitatory neurons, including those involved in breathing, interoception, and arousal, which depend on *Atoh1* expression in the RL as well (Rose at al., 2009). Thus, it is likely that auditory/vestibular nuclei deficits that we observed in *Lmx1a/b* DKO embryos, are part of a broader phenotype that includes defects in multiple dorsally-derived neuronal populations, resulting from the loss of *Atoh1* in the RL due to the disruption of roof plate function in these mutants.

In *Lmx1a/b* double mutants, inner ear central projections aberrantly populate the dorsal midline.

Inner ear afferents enter the hindbrain in r4 and extend anteriorly and posteriorly, without crossing the dorsal midline, to unilaterally innervate their corresponding nuclei (Duncan et al., 2019). In both auditory and other sensory systems, central projection formation is a tightly regulated process that is significantly independent from the formation of peripheral sensory epithelia and the corresponding brain nuclei (Fritzsch et al., 2019). For example, auditory spiral ganglion neurons can project into the hindbrain without either OC or cochlear nuclei development (Elliott et al., 2017; Fritzsch et al., 2019). Combined loss of *Lmx1a/b*, however, eliminated labeling of spiral ganglion neurons in our dye experiments and ablated OC and excitatory cochlear nuclei neurons, preventing the analysis of auditory central projections. In contrast, central vestibular projections still formed but showed massive reorganization in *Lmx1a/b* DKO mice. After entering the hindbrain, rather than forming longitudinal projections along the vestibular nuclei, in *Lmx1a/b* DKO embryos, inner ear vestibular afferents projected to the undifferentiated roof plate, overlaying the trigeminal and solitary tract fibers that aberrantly targeted the roof plate as well.

In situ hybridization failed to detect expression of *Lmx1a* in ganglion neurons during mouse embryonic development (Huang et al., 2008), suggesting that inner ear central projection pathfinding defects in *Lmx1a/b* DKO embryos result from the disruption of non-autonomous signaling, possibly signaling that involves secreted Wnt molecules. Mammals have 19 Wnts and several Wnt receptors, which have both redundant and unique functions during development (Rao and Kühl, 2010). Previous studies supported the targeting of inner ear afferents to a Wnt source in the dorsal hindbrain, at least partially via Fzd3 receptor (Duncan et al., 2019). Wnt3a, known to activate Wnt signaling via Fzd3 (Endo et al., 2008; Simonetti et al., 2014), is expressed in the lower RL, the dorsal-most region of the hindbrain neuroepithelium, but not in the roof plate or its later derivative, the choroid plexus (Parr et al., 1993; Hatch et al., 2007). Interestingly, inner ear neurons show a gradient of *Fzd3* expression. Those that express *Fzd3* at a moderate level terminate afferents within the

dorsal-most (*Wnt3a*-expressing) hindbrain, while those with high *Fzd3* expression terminate afferents at more ventral positions, before reaching the highest concentration of secreted Wnt molecules. Reducing Wnt reception by knocking out *Fzd3* shifts afferents, that normally terminate adjacent to the Wnt-expression domain, dorsally, suggesting that inner ear afferents stop dorsal expansion once they achieve a high level of Wnt signaling (Duncan et al., 2019; Yang et al., 2017).

In *Lmx1a/b* DKO embryos, at the level of otic vesicles, where inner ear afferents enter the hindbrain, *Wnt3a* expression appeared in the dorsal midline roof plate, which became populated by inner ear (vestibular) central projections. Consistent with the lack of posterior expansion of inner ear afferents, virtually no *Wnt3a* expression was detected in the hindbrain posterior to otic vesicles in *Lmx1a/b* DKO mice. Together, these data suggest that *Lmx1a/b* function in the roof plate is required to exclude *Wnt3a* expression from the roof plate/choroid plexus epithelium but establish it in the adjacent RL to navigate pathfinding of inner ear afferents to create an appropriate sensory map. Interestingly, in the spinal cord, in the absence of *Lmx1a*, rather than extending ventrally, axons of dI1 dorsal interneurons aberrantly target the roof plate, and axons of mechanoreceptor neurons do not properly expand along the anterior-posterior axis (Millen et al. 2004; Kridsada et al. 2018), suggesting the roof plate as a major regulator of neuronal projections throughout the central nervous system.

Although changes in *Wnt3a* expression is an attractive explanation for the *Lmx1a/b* DKO guidance deficits, our study does not exclude a possibility that other roof plate-derived secreted molecules also contribute to innervation defects in these mutants. Similarly, it is likely that big changes in the environment, such as changes in sensory organ size, composition, and availability, contribute to guidance errors in *Lmx1a/b* DKO mice as well.

The aberrant anterior expansion of trigeminal fibers to the cerebellum could be secondary to cerebellar defects in *Lmx1a/b* DKO mice (Mishima *et al.* 2009; Marzban *et al.* 2019).

Lmx1a/b redundantly regulate inner ear neurosensory development.

Loss of *Lmx1a* results in the disruption of boundary formation between sensory and non-sensory domains in the ear. Although abnormally sized, both vestibular and auditory sensory epithelia, however, are still present in *Lmx1a* mutant mice (Nichols et al. 2008; Koo et al. 2009; Steffes et al. 2012; Mann et al. 2017; Huang et al. 2018; Nichols et al. 2020). Loss of *Lmx1b* alone does not significantly alter auditory inner ear development (this study). In contrast, combined deletion of *Lmx1a/b* prevents auditory OC development and disrupts spiral ganglia, going beyond the limited effect of either *Lmx1a* or *Lmx1b* single-gene mutations (Fig. 10). Our conclusion regarding the lack of OC in *Lmx1a/b* DKO embryos is based on the lack of Myo7a immunostaining (a marker and an important regulator of hair cell development) in cochlea and the absence of cochlear innervation, revealed by α-Tubulin immunohistochemistry and lipophilic dye labeling (Fig. 3E, F, E”’; 3A, D; Fig. 2A, A’, D, D’).

In the developing mouse inner ear, *Lmx1a* and *Lmx1b* are expressed in largely non-overlapping pattern: *Lmx1a* - in non-sensory domains, while *Lmx1b* - in sensory cells.

Short-term fate mapping studies, however, revealed that at least some sensory cells originate from progenitors that expressed *Lmx1a*, suggesting that sensory epithelia defects in *Lmx1a/b* DKO embryos involve both cell-autonomous and non-autonomous mechanisms, which, possibly, converge on transcription factors critical for inner ear development. Interestingly, lack of cochlear development and spiral ganglion dye labeling in *Lmx1a/b* DKO mice resembles the phenotypes of *Pax2−/−* mice (Bouchard et al. 2010). In early *Lmx1a/b* DKO embryos, we observed a significant downregulation of Pax2 expression in the inner ear epithelium compared to control and *Lmx1a/b* single-gene mutants, suggesting that cochlear and spiral ganglion defects in *Lmx1a/b* double mutants are at least partially mediated by downregulated *P*ax2. Of note, otocysts-resembling inner ears of late *Lmx1a/b* DKO embryos are more severely affected than those in *Pax2−/−* mice, being somewhat more similar to the phenotype of mice with a delayed *Sox2* deletion (Dvorakova et al., 2020) or *Gata3−/−* mice (Duncan and Fritzsch, 2013), suggesting *Sox2* and *Gata3* as potential *Lmx1a/b* downstream candidate genes in inner ear development as well. Also, spiral and vestibular ganglia defects in *Lmx1a/b* DKO mutants could be secondary to overall changes in the double mutant environment, such as alterations in sensory epithelia, brainstem nuclei, and/or roof plate signaling.

In conclusion, we showed that development of the inner ear, central projections, and brainstem cochlear/vestibular nuclei redundantly depend on *Lmx1a/b*. Our data suggest that *Lmx1a/b* regulate inner ear auditory development, at least partially, by regulating expression of *Pax2*, while brainstem nuclei and central projection pathfinding defects in *Lmx1a/b* DKO mice likely result from roof plate-dependent disruption of *Wnt3a* and *Atoh1* expression in the RL. Future analysis of conditional *Lmx1a/b* knockouts in specific cellular populations is needed to more precisely dissect the origin and underlying mechanisms of the reported phenotypes.

Acknowledgments:

We thank R. Johnson (MD Anderson Cancer Center) for providing the *Lmx1b* knockout mice and A. Clarke (UTHSC) for helpful comments on the manuscript. This work was supported by NIH grants R01 DC005590 and AG060504 (to BF), R01 NS093009 (to VC) and the Neuroscience Institute of the UTHSC.

References:

Abello G, Khatri S, Radosevic M, Scotting P, Giraldez F, Alsina B (2010) Independent regulation of Sox3 and Lmx1b by FGF and BMP signaling influences the neurogenic and non-neurogenic domains in the chick otic placode. Developmental Biology 339:166–178. [PubMed: 20043898]

Boëda B, El-Amraoui A, Bahloul A, Goodyear R, Daviet L, Blanchard S, Perfettini I, Fath KR, Shorte S, Reiners J, Houdusse A, Legrain P, Wolfrum U, Richardson G, Petit C (2002) Myosin VIIa, harmonin and cadherin 23, three Usher I gene products that cooperate to shape the sensory hair cell bundle. EMBO J 21:6689–99. [PubMed: 12485990]

Bouchard M, de Caprona D, Busslinger M, Xu P, Fritzsch B (2010) Pax2 and Pax8 cooperate in mouse inner ear morphogenesis and innervation. BMC Developmental Biology 10:89. [PubMed: 20727173]

Butts T, Green MJ, Wingate RJ (2014) Development of the cerebellum: simple steps to make a ‘little brain’. Development 141:4031–4041. [PubMed: 25336734]

Chang C-H, Tsai R-K, Tsai M-H, Lin Y-H, Hirobe T (2014) The roles of Frizzled-3 and Wnt3a on melanocyte development: in vitro studies on neural crest cells and melanocyte precursor cell lines. Journal of Dermatological Science 75:100–108. [PubMed: 24815018]

Chen H, Lun Y, Ovchinnikov D, Kokubo H, Oberg KC, Pepicelli CV, Can L, Lee B, et al. (1998) Limb and kidney defects in Lmx1b mutant mice suggest an involvement of LMX1B in human nail patella syndrome. Nature Genetics 19:51–55. [PubMed: 9590288]

Chizhikov VV, Lindgren AG, Currle DS, Rose MF, Monuki ES et al. (2006) The roof plate regulates cerebellar cell-type specification and proliferation. Development 133:2793–2804. [PubMed: 16790481]

Chizhikov VV, Lindgren AG, Mishima Y, Roberts RW, Aldinger KA et al. (2010) Lmx1a regulates fates and location of cells originating from the cerebellar rhombic lip and telencephalic cortical hem. Proceedings of the National Academy of Sciences 107:10725–10730.

Chizhikov VV, Iskusnykh IY, Steshina EY, Lindgren AG, Shetty AS et al. (2019) Early dorsomedial tissue interactions regulate gyrification of distal neocortex. Nature Commun 10:5192. [PubMed: 31729356]

Di Bonito M, Studer M, Puelles L (2017) Nuclear derivatives and axonal projections originating from rhombomere 4 in the mouse hindbrain. Brain Structure and Function 222:3509–3542. [PubMed: 28470551]

Doucet-Beaupré H, Ang SL, Lévesque M (2015) Cell fate determination, neuronal maintenance and disease state: The emerging role of transcription factors Lmx1a and Lmx1b. FEBS Lett 589:3727–38. [PubMed: 26526610]

Duncan JS, Fritzsch B (2013) Continued expression of GATA3 is necessary for cochlear neurosensory development. PloS One 8:e62046. [PubMed: 23614009]

Duncan JS, Fritzsch B, Houston DW, Ketchum EM, Kersigo J, Deans MR, Elliott KL (2019) Topologically correct central projections of tetrapod inner ear afferents require Fzd3. Scientific Reports 9:10298. [PubMed: 31311957]

Dvorakova M, Macova I, Bohuslavova R, Anderova M, Fritzsch B, Pavlinkova G (2020) Early ear neuronal development, but not olfactory or lens development, can proceed without SOX2. Dev Biol 457:43–56. [PubMed: 31526806]

Elliott KL, Kersigo J, Pan N, Jahan I, Fritzsch B (2017) Spiral Ganglion Neuron Projection Development to the Hindbrain in Mice Lacking Peripheral and/or Central Target Differentiation. Frontiers in Neural Circuits 11:25. [PubMed: 28450830]

Elliott KL, Fritzsch B (2018) Ear transplantations reveal conservation of inner ear afferent pathfinding cues. Scientific Reports 8:13819. [PubMed: 30218045]

Endo Y, Beauchamp E, Woods D, Taylor WG, Toretsky JA, Üren A, Rubin JS (2008) Wnt-3a and Dickkopf-1 stimulate neurite outgrowth in Ewing tumor cells via a Frizzled3-and c-Jun N-terminal kinase-dependent mechanism. Molecular and Cellular Biology 28:2368–2379. [PubMed: 18212053]

Farago AF, Awatramani RB, Dymecki SM (2006) Assembly of the brainstem cochlear nuclear complex is revealed by intersectional and subtractive genetic fate maps. Neuron 50:205–218. [PubMed: 16630833]

Filova I, Dvorakova M, Bohuslavova R, Pavlinek A, Elliott KL, Vochyanova S, Fritzsch B, Pavlinkova G (2020) Combined Atoh1 and Neurod1 Deletion Reveals Autonomous Growth of Auditory Nerve Fibers. Molecular Neurobiology 57:5307–5323. [PubMed: 32880858]

Fritzsch B, Nichols D (1993) DiI reveals a prenatal arrival of efferents at the differentiating otocyst of mice. Hearing research 65:51–60. [PubMed: 8458759]

Fritzsch B, Pauley S, Feng F, Matei V, Nichols D (2006) The molecular and developmental basis of the evolution of the vertebrate auditory system. International Journal of Comparative Psychology 19:1–25.

Fritzsch B, Pan N, Jahan I, Duncan JS, Kopecky BJ, Elliott KL, Kersigo J, Yang T (2013) Evolution and development of the tetrapod auditory system: an organ of Corti-centric perspective. Evolution & Development 15:63–79. [PubMed: 23331918]

Fritzsch B and Elliott KL (2017) Gene, cell, and organ multiplication drives inner ear evolution. Dev Biol. 431:3–15. [PubMed: 28866362]

Fritzsch B, Elliott KL, Pavlinkova G (2019) Primary sensory map formations reflect unique needs and molecular cues specific to each sensory system. F1000Research 8: F1000 Faculty Rev-345.

Fujiyama T, Yamada M, Terao M, Terashima T, Hioki H, Inoue YU, Inoue T, Masuyama N, et al. (2009) Inhibitory and excitatory subtypes of cochlear nucleus neurons are defined by distinct bHLH transcription factors, Ptf1a and Atoh1. Development 136:2049–2058. [PubMed: 19439493]

Glover JC, Elliott KL, Erives A, Chizhikov VV, Fritzsch B (2018) Wilhelm His' lasting insights into hindbrain and cranial ganglia development and evolution. Developmental Biology 444:S14–S24. [PubMed: 29447907]

Gordy C, Straka H, Houston DW, Fritzsch B, Elliott KL (2018) Transplantation of Ears Provides Insights into Inner Ear Afferent Pathfinding Properties. Developmental Neurobiology 78:1064–1080. [PubMed: 30027559]

Grandi FC, De Tomasi L, Mustapha M. (2020) Single-Cell RNA Analysis of Type I Spiral Ganglion Neurons Reveals a Lmx1a Population in the Cochlea. Front Mol Neurosci 13:83. [PubMed: 32523514]

Grati M, Kachar B, 2011 Myosin VIIa and sans localization at stereocilia upper tip-link density implicates these Usher syndrome proteins in mechanotransduction. Proc Natl Acad Sci U S A. 108:11476–81. [PubMed: 21709241]

Grothe B, Carr CE, Casseday JH, Fritzsch B, Köppl C (2004) The evolution of central pathways and their neural processing patterns In: Evolution of the vertebrate auditory system, vol., pp. 289–359. Springer.

Hatch EP, Noyes CA, Wang X, Wright TJ, Mansour SL (2007) Fgf3 is required for dorsal patterning and morphogenesis of the inner ear epithelium. Development 134:3615–3625. [PubMed: 17855431]

Huang M, Sage C, Li H, Xiang M, Heller S, Chen ZY (2008) Dev Dyn 237:3305–12. [PubMed: 18942141]

Huang Y, Hill J, Yatteau A, Wong L, Jiang T, Petrovic J, Gan L, Dong L, et al. (2018) Reciprocal negative regulation between Lmx1a and Lmo4 is required for inner ear formation. Journal of Neuroscience 38:2484–2417.

Iskusnykh IY, Steshina EY, Chizhikov VV (2016) Loss of Ptf1a leads to a widespread cell-fate misspecification in the brainstem, affecting the development of somatosensory and viscerosensory nuclei. Journal of Neuroscience 36:2691–2710. [PubMed: 26937009]

Iskusnykh IY, Buddington RK, Chizhikov VV (2018) Preterm birth disrupts cerebellar development by affecting granule cell proliferation program and Bergmann glia. Exp Neurol. 306:209–221. [PubMed: 29772246]

Kersigo J, D'Angelo A, Gray BD, Soukup GA, Fritzsch B (2011) The role of sensory organs and the forebrain for the development of the craniofacial shape as revealed by Foxg1-cre-mediated microRNA loss. Genesis 49:326–341. [PubMed: 21225654]

Kim YY, Nam H, Jung H, Kim B, Suh JG, 2017 Over-expression of myosin7A in cochlear hair cells of circling mice. Lab Anim Res. 33:1–7. [PubMed: 28400833]

Koo SK, Hill JK, Hwang CH, Lin ZS, Millen KJ, Wu DK (2009) Lmx1a maintains proper neurogenic, sensory, and non-sensory domains in the mammalian inner ear. Developmental Biology 333:14–25. [PubMed: 19540218]

Kridsada K, Niu J, Haldipur P, Wang Z, Ding L, Li JJ, Lindgren AG, Herrera E, et al. (2018) Roof plate-derived radial glial-like cells support developmental growth of rapidly adapting mechanoreceptor ascending axons. Cell Reports 23:2928–2941. [PubMed: 29874580]

Landsberg RL, Awatramani RB, Hunter NL, Farago AF, DiPietrantonio HJ, Rodriguez CI, Dymecki SM (2005) Hindbrain rhombic lip is comprised of discrete progenitor cell populations allocated by Pax6. Neuron. 48:933–47. [PubMed: 16364898]

Lee SY, Han JH, Carandang M, Kim MY, Kim B, Yi N, Kim J, Kim BJ, Oh DY, Koo JW, Lee JH, Oh SH, Choi BY (2020) Novel genotype-phenotype correlation of functionally characterized LMX1A variants linked to sensorineural hearing loss. Hum Mutat. 41:1877–83. [PubMed: 32840933]

Lipovsek M, Wingate RJ (2018) Conserved and divergent development of brainstem vestibular and auditory nuclei. eLife 7:e40232. [PubMed: 30566077]

Machold R, Fishell G (2005) Math1 is expressed in temporally discrete pools of cerebellar rhombic-lip neural progenitors. Neuron 48:17–24. [PubMed: 16202705]

Macova I, Pysanenko K, Chumak T, Dvorakova M, Bohuslavova R, Syka J, Fritzsch B, Pavlinkova G (2019) Neurod1 is essential for the primary tonotopic organization and related auditory information processing in the midbrain. Journal of Neuroscience 39:984–1004. [PubMed: 30541910]

Maklad A, Kamel S, Wong E, Fritzsch B (2010) Development and organization of polarity-specific segregation of primary vestibular afferent fibers in mice. Cell Tissue Res 340:303–321. [PubMed: 20424840]

Mann ZF, Galvez H, Pedreno D, Chen Z, Chrysostomou E, Żak M, Kang M, Canden E, et al. (2017) Shaping of inner ear sensory organs through antagonistic interactions between Notch signalling and Lmx1a. Elife 6:e33323. [PubMed: 29199954]

Mao Y, Reiprich S, Wegner M, Fritzsch B (2014) Targeted deletion of Sox10 by Wnt1-cre defects neuronal migration and projection in the mouse inner ear. PloS one 9:e94580. [PubMed: 24718611]

Marzban H, Rahimi-Balaei M, Hawkes R (2019) Early trigeminal ganglion afferents enter the cerebellum before the Purkinje cells are born and target the nuclear transitory zone. Brain Structure and Function 224:2421–2436. [PubMed: 31256239]

Millen K, Millonig J, Hatten M (2004) Roof plate and dorsal spinal cord dl1 interneuron development in the dreher mutant mouse. Developmental Biology 270:382–392. [PubMed: 15183721]

Millonig JH, Millen KJ, Hatten ME (2000) The mouse Dreher gene Lmx1a controls formation of the roof plate in the vertebrate CNS. Nature 403:764. [PubMed: 10693804]

Mishima Y, Lindgren AG, Chizhikov VV, Johnson RL, Millen KJ (2009) Overlapping function of Lmx1a and Lmx1b in anterior hindbrain roof plate formation and cerebellar growth. Journal of Neuroscience 29:11377–11384. [PubMed: 19741143]

Nichols DH, Bouma JE, Kopecky BJ, Jahan I, Beisel KW, He DZZ, Liu H, Fritzsch B (2020) Interaction with ectopic cochlear crista sensory epithelium disrupts basal cochlear sensory epithelium development in Lmx1a mutant mice. Cell Tissue Res 380:435–448. [PubMed: 31932950]

Nichols DH, Pauley S, Jahan I, Beisel KW, Millen KJ, Fritzsch B (2008) Lmx1a is required for segregation of sensory epithelia and normal ear histogenesis and morphogenesis. Cell Tissue Res 334:339–358. [PubMed: 18985389]

Nothwang HG (2016) Evolution of mammalian sound localization circuits: A developmental perspective. Progress in neurobiology 141:1–24. [PubMed: 27032475]

Parr BA, Shea MJ, Vassileva G, McMahon AP (1993) Mouse Wnt genes exhibit discrete domains of expression in the early embryonic CNS and limb buds. Development 119:247–261. [PubMed: 8275860]

Rao TP, Kühl M (2010) An updated overview on Wnt signaling pathways: a prelude for more. Circulation Research 106:1798–1806. [PubMed: 20576942]

Rose MF, Ahmad KA, Thaller C, Zoghbi HY, 2009 Excitatory neurons of the proprioceptive, interoceptive, and arousal hindbrain networks share a developmental requirement for Math1. Proc Natl Acad Sci U S A. 106: 22462–7. [PubMed: 20080794]

Sanchez-Guardado LO, Puelles L, Hidalgo-Sanchez M, 2019 Origin of acoustic-vestibular ganglionic neuroblasts in chick embryos and their sensory connections. Brain Struct Funct. 224:2757–2774. [PubMed: 31396696]

Schmidt H, Fritzsch B (2019) Npr2 null mutants show initial overshooting followed by reduction of spiral ganglion axon projections combined with near-normal cochleotopic projection. Cell Tissue Res 378:15–32. [PubMed: 31201541]

Schrauwen I, Chakchouk I, Liaqat K, Jan A, Nasir A, Hussain S, Nickerson DA, Bamshad MJ, et al. (2018) A variant in LMX1A causes autosomal recessive severe-to-profound hearing impairment. Human Genetics 137:471–478. [PubMed: 29971487]

Sieber C, Kopf J, Hiepen C, Knaus P (2009) Recent advances in BMP receptor signaling. Cytokine & Growth Factor Reviews 20:343–355. [PubMed: 19897402]

Sienknecht UJ, Köppl C and Fritzsch B, 2014 Evolution and development of hair cell polarity and efferent function in the inner ear. Brain, Behavior and Evolution 83: 150–161.

Simonetti M, Agarwal N, Stösser S, Bali KK, Karaulanov E, Kamble R, Pospisilova B, Kurejova M, et al. (2014) Wnt-Fzd signaling sensitizes peripheral sensory neurons via distinct noncanonical pathways. Neuron 83:104–121. [PubMed: 24991956]

Steffes G, Lorente-Cánovas B, Pearson S, Brooker RH, Spiden S, Kiernan AE, Guénet J-L, Steel KP (2012) Mutanlallemand (mtl) and Belly Spot and Deafness (bsd) are two new mutations of Lmx1a causing severe cochlear and vestibular defects. PloS One 7:e51065. [PubMed: 23226461]

Wang VY, Rose MF, Zoghbi HY (2005) Math1 expression redefines the rhombic lip derivatives and reveals novel lineages within the brainstem and cerebellum. Neuron 48:31–43. [PubMed: 16202707]

Wesdorp M, de Koning Gans PAM, Schraders M, Oostrik J, Huynen MA, Venselaar H, Beynon AJ, van Gaalen J, et al. (2018) Heterozygous missense variants of LMX1A lead to nonsyndromic hearing impairment and vestibular dysfunction. Human Genetics 137: 389–400. [PubMed: 29754270]

Yang T, Kersigo J, Wu S, Fritzsch B, Bassuk AG (2017) Prickle1 regulates neurite outgrowth of apical spiral ganglion neurons but not hair cell polarity in the murine cochlea. PloS One 12:e0183773. [PubMed: 28837644]

Highlights

- Combined loss of *Lmx1a/b* disrupts auditory inner ear development, preventing formation of the organ of Corti.
- Loss of *Lmx1a* and *Lmx1b* leads to milder inner ear vestibular innervation abnormalities.
- In *Lmx1a/b* double mutants, vestibular afferents aberrantly project to the hindbrain dorsal midline.
- Combined loss of *Lmx1a/b* prevents the development of excitatory neurons of cochlear and vestibular nuclei.

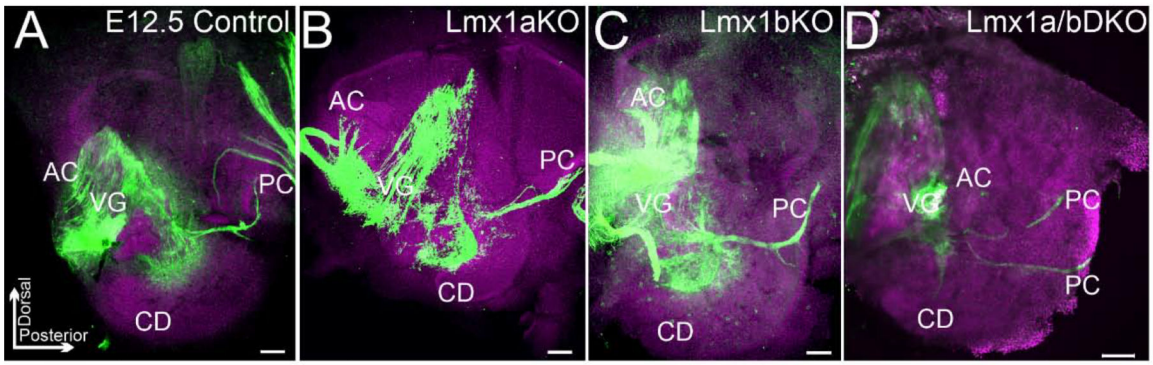

Fig. 1. Auditory and vestibular inner ear innervation abnormalities of *Lmx1a/b* DKO embryos at e12.5.

Whole inner ear innervation in e12.5 embryos revealed by anti-acetylated α-Tubulin immunohistochemistry (green) combined with Hoechst nuclear stain (lilac).

Posterior canal crista (PC) innervation appeared as a single branch in control (A), *Lmx1a* KO (B), and *Lmx1b* KO (C) embryos but consisted of two branches in *Lmx1a/b* DKO embryos (D). Innervation toward anterior/horizontal cristae (labeled as AC – anterior crista) and cochlear duct (CD) was clearly detectable in control, *Lmx1a* KO and *Lmx1b* KO embryos (A-C). Innervation toward AC was poorly developed and no CD innervation was detected in *Lmx1a/b* DKO embryos (D). VG - vestibular ganglion.

Orientation is given in panel A. Scale bar: 100 μm.

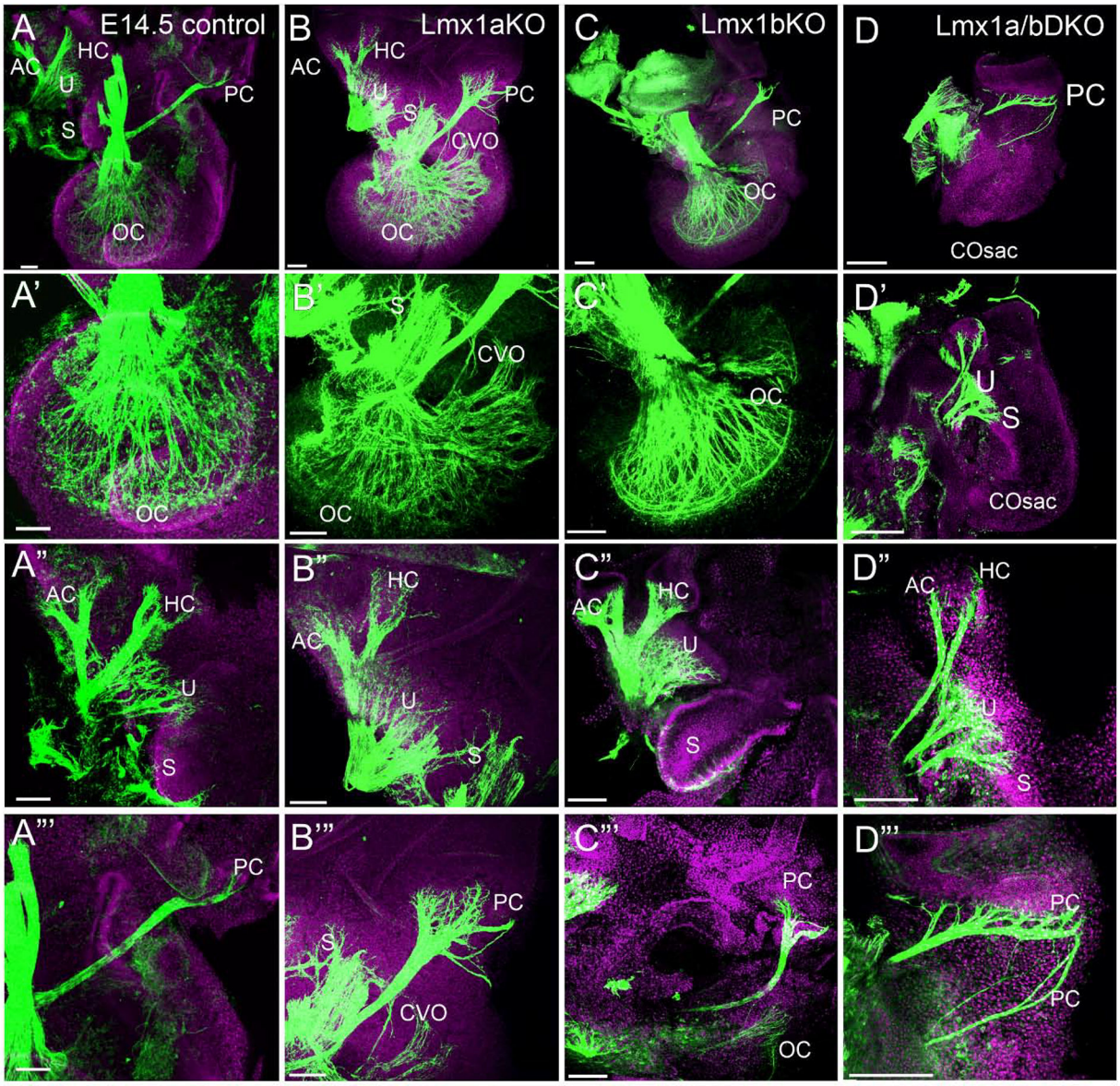

Fig. 2. Auditory and vestibular inner ear innervation abnormalities of *Lmx1a/b* DKO embryos at e14.5.

Anti-acetylated α-Tubulin immunostaining (green) in the inner ear of indicated genotypes. Some samples were co-stained with Hoechst nuclear stain (lilac) to visualize tissue.

Panels A-D show innervation in the entire inner ear at low magnification; panels A'-D' show auditory inner ear innervation at higher magnification; panels A"- D" and A"'- D"' show vestibular inner ear innervation at higher magnification.

(A-D') Organ of Cori (OC) innervation was clearly detectable in control, *Lmx1a* KO and *Lmx1b* KO embryos (A-C, A'-C') but no cochlear innervation was found in *Lmx1a/b* DKO embryos, in which a cochlear sac (COSac) formed (D, D'). Consistent with previously described partial transformation of the OC into an irregular vestibular epithelium (NICHOLS et al., 2008), innervation to an abnormal cochlear-vestibular organ (CVO) was detected in *Lmx1a* KO mice (B, B').

(A”-D”) In *Lmx1a/b* DKO mice, branches innervating anterior crista (AC) and horizontal crista (HC) appeared abnormally thin compared to control, *Lmx1a* KO and *Lmx1b* KO ears. Some innervation to utricle (U) and saccule (S) was present in *Lmx1a* KO, *Lmx1b* KO and *Lmx1a/b* DKO ears.
(A”’-D”’) Innervation of posterior crista (PC) appeared extended in *Lmx1a* KO and *Lmx1a/b* DKO embryos, consisting of multiple small branches in *Lmx1a* KO and multiple large branches in *Lmx1a/b* DKO mutants.
Scale bar: 100 μm for all images.

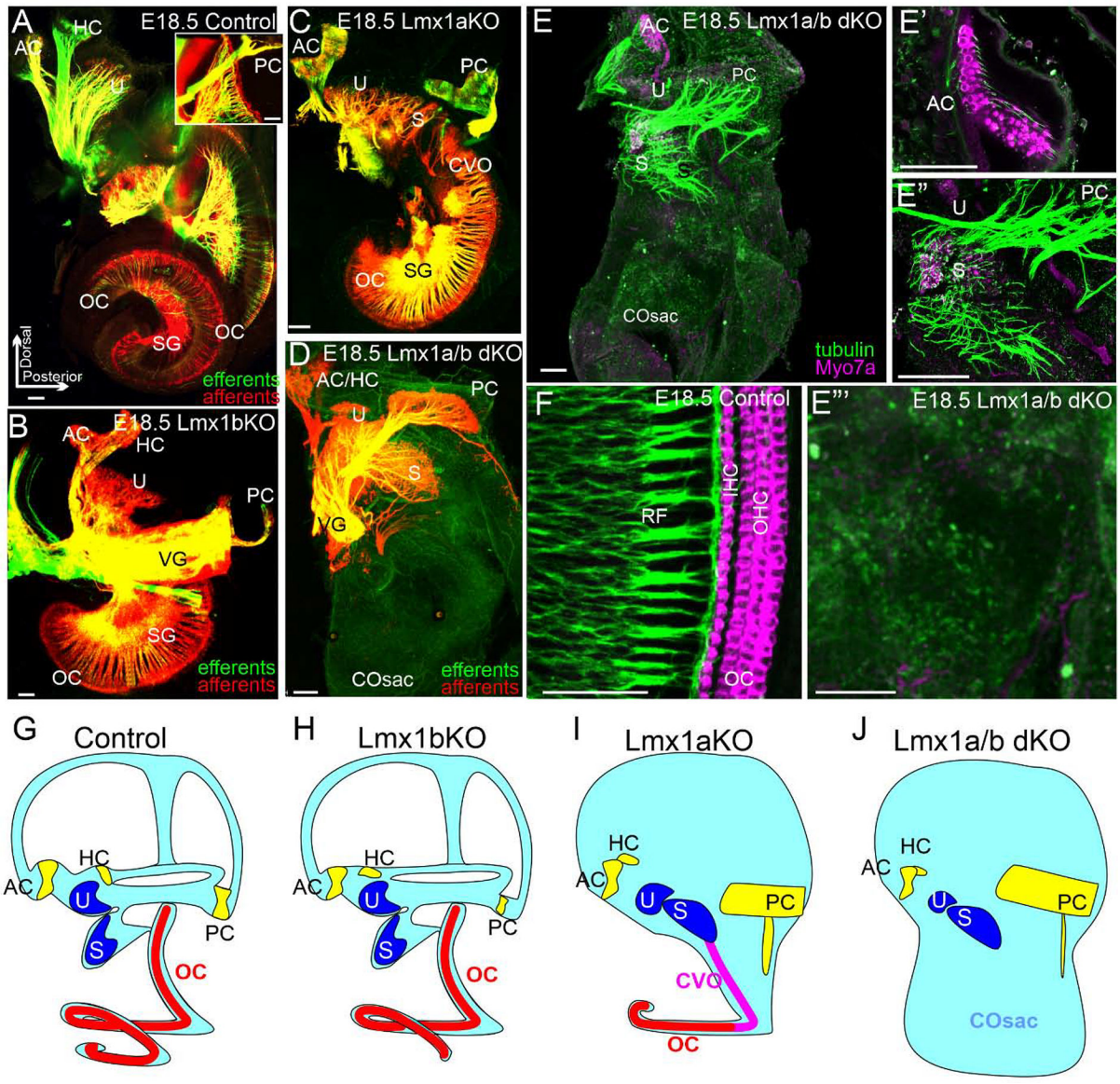

Fig. 3. Lack of organ of Corti and spiral ganglion, and milder vestibular inner ear abnormalities in *Lmx1a/b* DKO embryos at e18.5.

(A-D) Dye tracing of afferents (red) and efferents (green) in the inner ear of indicated genotypes. In e18.5 *Lmx1b* KO inner ears, dye tracing revealed all auditory (organ of Corti - OC, spiral ganglion - SG) and vestibular (anterior canal crista - AC, horizontal canal crista - HC, posterior canal crista - PC, utricle - U, saccule - S) components. A reduced PC innervation and partially fused AC/HC innervation, however, was observed in *Lmx1b* KO embryos compared to controls (A, B). VG - vestibular ganglion.

In *Lmx1a* KO embryos, innervation to AC/HC was partially fused, innervation to PC showed excessive branching, and innervation to saccule (S) was fused with OC, forming an abnormal cochlear-vestibular organ (CVO) (C). *Lmx1a/b* DKO ears lacked the innervation of OC and SG labeling. Innervation to AC/HC was partially fused, innervation to U was

reduced, while innervation to PC was increased with excessive branching and abnormal ventral expansion of fibers (D).

(E-F) Anti-acetylated α-Tubulin (green)/anti-Myo7 (magenta) double immunohistochemistry. (E) Low magnification image showing the entire e18.5 *Lmx1a/b* DKO inner ear. (E', E") High magnification of vestibular components of e18.5 *Lmx1a* DKO inner ear. Myo7a labeling of hair cells confirmed that vestibular sensory epithelia (AC, U, S) still formed in appropriate places in the *Lmx1a/b* DKO inner ear (E-E"). (F) High magnification image of OC in e18.5 control inner ear, showing properly arranged Myo7a+ outer hair cells (OHC) and inner hair cells (IHC), innervated by radial fibers (RF). (E"') High magnification e18.5 *Lmx1a/b* DKO cochlear sac (COsac), which lacked OC based on the absence of both Myo7a labeling and tubulin+ RF.

(G-J) Schematics summarizing inner ear abnormalities in *Lmx1a/b* single and double mutants.

Orientation is given in panel A. Scale bar: 100 μm for all images.

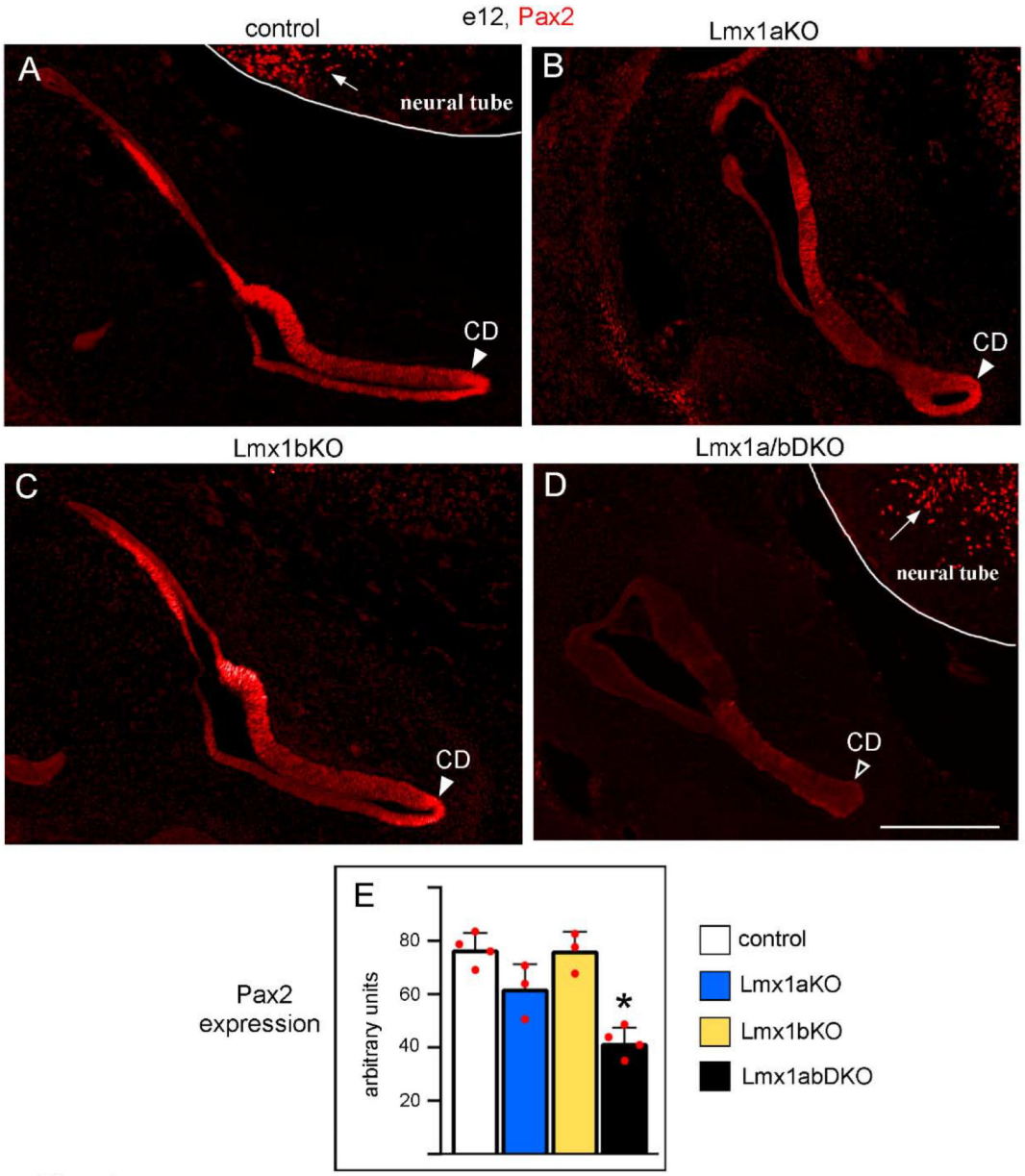

Fig. 4. Simultaneous but not individual loss of *Lmx1a* and *Lmx1b* reduces *Pax2* expression in the inner ear.

Transverse sections of the e12 inner ear immunostained with an anti-Pax2 antibody. *Pax2* was strongly expressed in the inner ear, including the developing cochlear duct (CD, arrowhead) in control (A), *Lmx1a* KO (B) and *Lmx1b* KO (C) embryos. *Pax2* expression appeared reduced in the inner ear, including the developing CD, of *Lmx1a/b* DKO embryos (D, open arrowhead). Note that *Pax2* was similarly expressed in the neural tube of *Lmx1a/b* DKO and control embryos (arrows in A and D) indicating that double loss of *Lmx1a* and *Lmx1b* reduced *Pax2* expression specifically in the ear. (E) Quantification of Pax2 immunostaining intensity revealed no statistically significant difference between control, *Lmx1a* KO and *Lmx1b* KO inner ears ($p>0.05$), but a reduction of Pax2 expression in the inner ear of L*mx1a/b DKO* embryos (asterisk) relative to control ($p<0.001$), *Lmx1a* KO

(p=0.014) and *Lmx1b* KO (p<0.001) embryos. n=4 control, n=3 *Lmx1a* KO, n=3 *Lmx1b KO*, and n=4 *Lmx1a/b* DKO embryos. Scale bar: 200 μm.

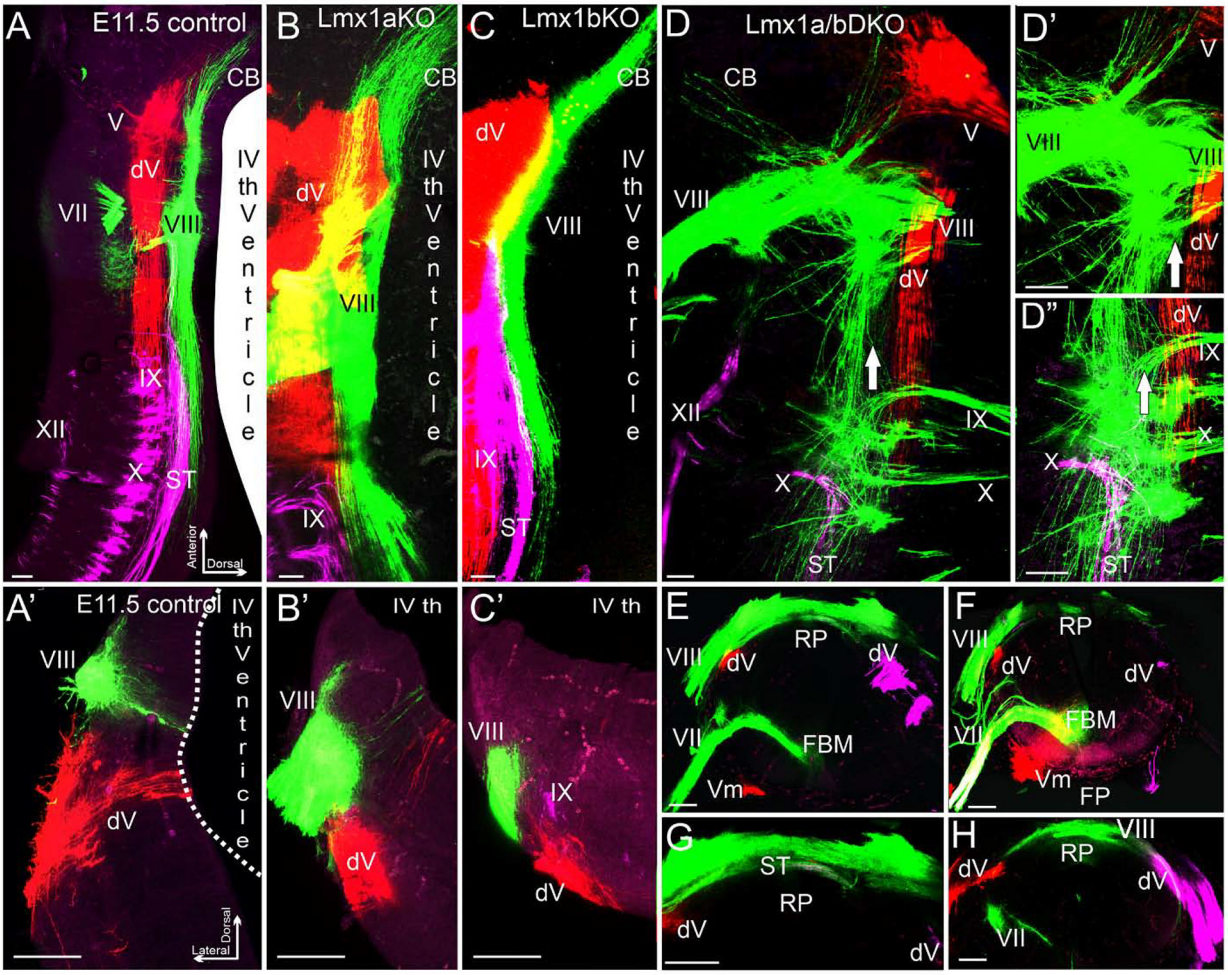

Fig. 5. Inner ear central vestibular projections aberrantly target the hindbrain roof plate in e11.5 *Lmx1a/b* DKO embryos.

Whole mounted hindbrains (A-D") and transverse hindbrain sections (A'-C', E-H) from e11.5 embryos of indicated genotypes. Discrete sensory afferent projections were visualized by labeling distinct cranial nerves (indicated by Roman numbers) with lipophilic dyes. V - trigeminal nerve, dV - descending trigeminal tract, VII - facial nerve, VIII – inner ear vestibular nerve, IX - glossopharyngeal nerve, X - vagus nerve, XII - hypoglossal nerve. (A-C, A'-C') In control, *Lmx1a* KO, and *Lmx1b* KO embryos, different afferent projections run parallel to the anterior-posterior axis of the hindbrain, do not significantly overlap with each other, and do not cross the dorsal midline occupied by the wide choroid plexus epithelium derived from the IVth ventricle roof plate.

(D-D") Dorsal whole mount view showing that in *Lmx1a/b* DKO embryos, inner ear vestibular (VIII), trigeminal (V), and solitary tract (ST) afferents extend aberrantly close to or cross the dorsal midline. Arrow (D-D") shows location of the dorsal midline, which is heavily populated by inner ear vestibular (VIII) afferent fibers. D' and D" are high power views of D.

(A'-C', E-H) Transverse hindbrain sections showing that similar to control, *Lmx1a* KO and *Lmx1b* KO embryos, in *Lmx1a/b* DKO hindbrain, the descending trigeminal tract (dV) was

located ventral to inner ear vestibular (VIII) fibers. However, in contrast to control, *Lmx1a* KO and *Lmx1b* KO embryos (A'-C'), inner ear vestibular (VIII) fibers extended to and populated the dorsal midline roof plate (RP) covering the central canal in *Lmx1a/b* DKO littermates (E-H). Note the near normal location of facial branchial motor neurons (FBM) and ventral motor neurons (Vm) in the *Lmx1a/b* DKO (E, F) near the floor plate (FP), and solitary tract afferents crossing the roof plate (G). G is a high power view of E, without the magenta channel; panels F and H show two different sections from another embryo. Scale bar: 100 μm.

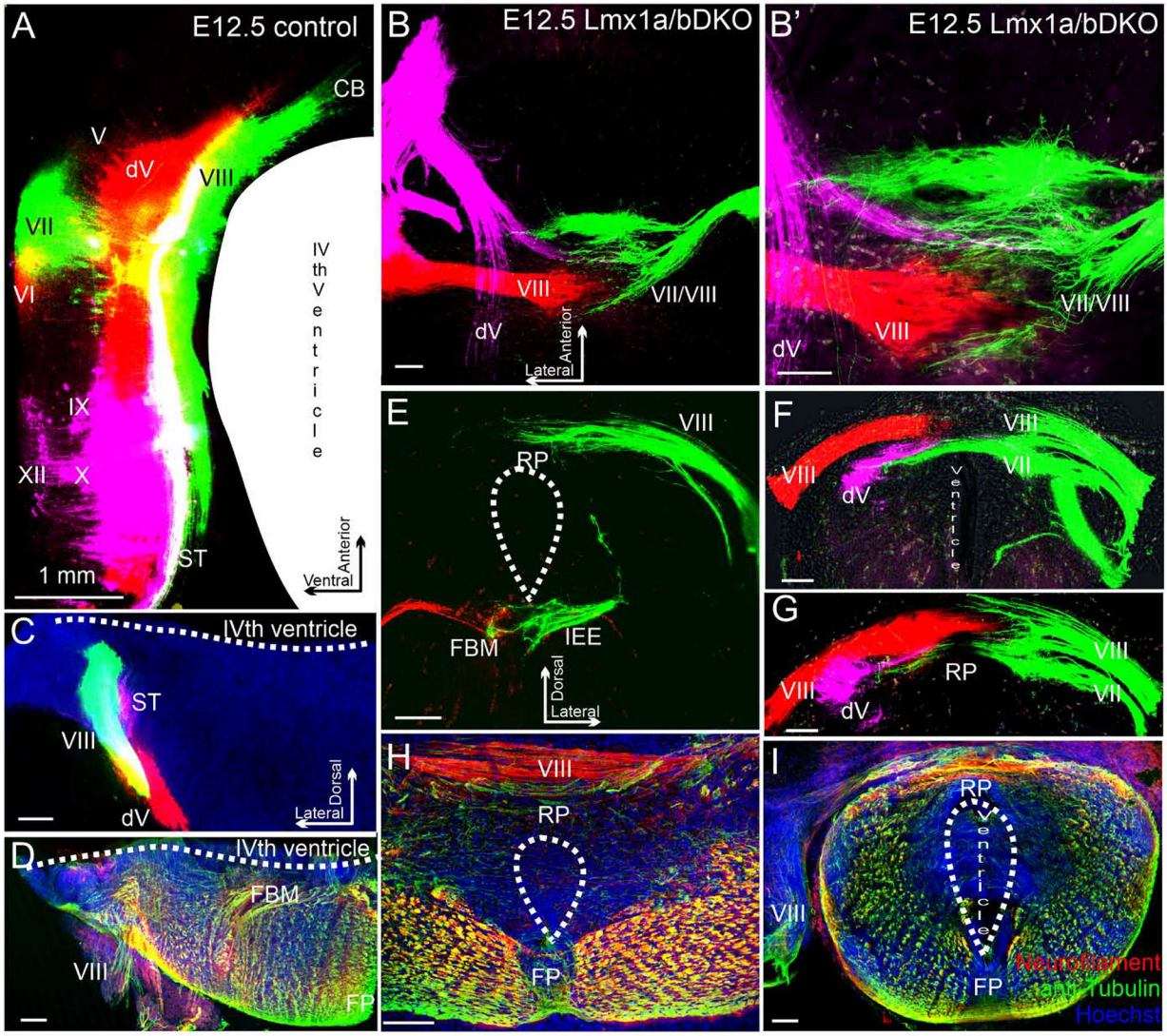

Fig. 6. In e12.5 *Lmx1a/b* DKO mutants, inner ear central projections from left and right ears interdigitate but do not fuse at the hindbrain dorsal midline.

Dorsal view of whole mount hindbrain (A-B') or transverse sections (C-I) of e12.5 embryos. Selected afferents were labeled with dye (A-C, E-G) or anti-Neurofilament/anti-acetylated α-Tubulin immunohistochemistry (D, H, I). Cranial nerves are indicated by Roman numbers. (A, C) Selected ipsilateral afferents labeled with dye (cranial nerves VII/VIII are green, nerves dV/VI are red, and nerves IX/X/XII are lilac. In control embryos, beyond r1-derived cerebellum (CB) (A), vestibular inner ear (cranial nerve VIII) and trigeminal (dV) projections do not come close to the dorsal midline.

(B-G) Labeling of the trigeminal (lilac), inner ear (red) and facial/inner ear projection from the opposite side (green) in a *Lmx1a/b* DKO embryo. B' shows higher magnification of B. Panels F and G show consecutive sections from the same embryo, Panel E shows a different embryo. All these nerves, after entering the brainstem, aberrantly extend across the roof plate (RP) that occupies the brainstem dorsal midline. Afferents from the two ears clearly interdigitate at the roof plate but do not fuse (B, B' F, G). In the double mutant, afferents of

the cranial nerve VII-derived solitary tract and trigeminal afferents cross the roof plate below the vestibular inner ear nerve VIII (F, G). In contrast to pathfinding errors of afferents that normally target the alar plate, facial branchial motor neurons (FBM) and inner ear efferents (IEE) were appropriately located in the basal plate of e12.5 *Lmx1a/b* DKO embryos (E). (D, H, I) In *Lmx1a/b* DKO mutants, fiber bundles crossing the roof plate can also be visualized using anti-Neurofilament (red)/anti-acetylated α-Tubulin (green) immunohistochemistry.

Hoechst counterstaining is blue (H, I). Panels H and I show sections from two different embryos. No comparably located fibers were detected in control embryos (D). Note that because the IV^{th} ventricle does not properly form in *Lmx1a/b* DKO embryos, the double mutant overall brainstem morphology is somewhat similar to the spinal cord (E-I).

Scale bars: 1 mm (A), 100 μm (all other panels).

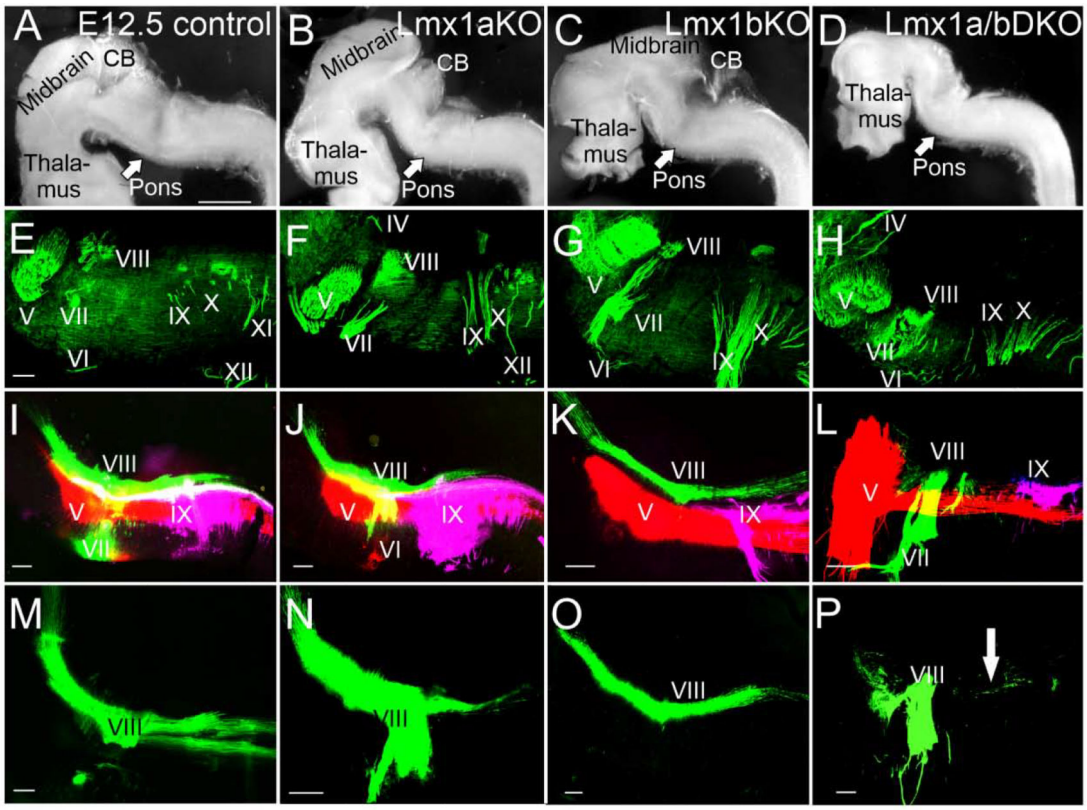

Fig. 7. Anterior-posterior expansion of inner ear central projections is disrupted in e12.5 *Lmx1a/b* DKO embryos.

In all panels, anterior is left, posterior is right, dorsal is up, ventral is down.

(A-D) Side view of dissected whole mount brains. Overall brainstem morphology is similar in control, *Lmx1a* KO and *Lmx1b* KO embryos (A-C). While the overall shape and size of the caudal brainstem show no obvious deviations in *Lmx1a/b* DKO embryos, their cerebellum (CB) and midbrain are reduced in size (D).

(E-H) Anti-Neurofilament immunohistochemistry shows the presence and appropriate location of all cranial nerve roots (V-XII) in *Lmx1a* KO, *Lmx1b* KO and *Lmx1a/b* DKO embryos, suggesting that overall anterior-posterior hindbrain patterning is not grossly disrupted in these mutants.

(I-P) Dye labeling of cranial nerve V (red), VII/VIII (green) and IX (lilac). Panels I-L show co-imaging of three different colors, while panels M-P – only green labeling to better visualize defects in vestibular (nerve VIII) projections. No gross deviation of overall projections in *Lmx1a* KO (J, N) and *Lmx1b* KO (K, O) embryos was detected compared to controls (I, M). In contrast, *Lmx1a/b* DKO embryos show limited posterior expansion of ear vestibular projections (nerve VIII) (L, P, arrow) and an abnormal trigeminal (nerve V) expansion into the topographical equivalent of r1/cerebellum (L).

Scale bars: 1mm (A-D), 100 μm (E-P).

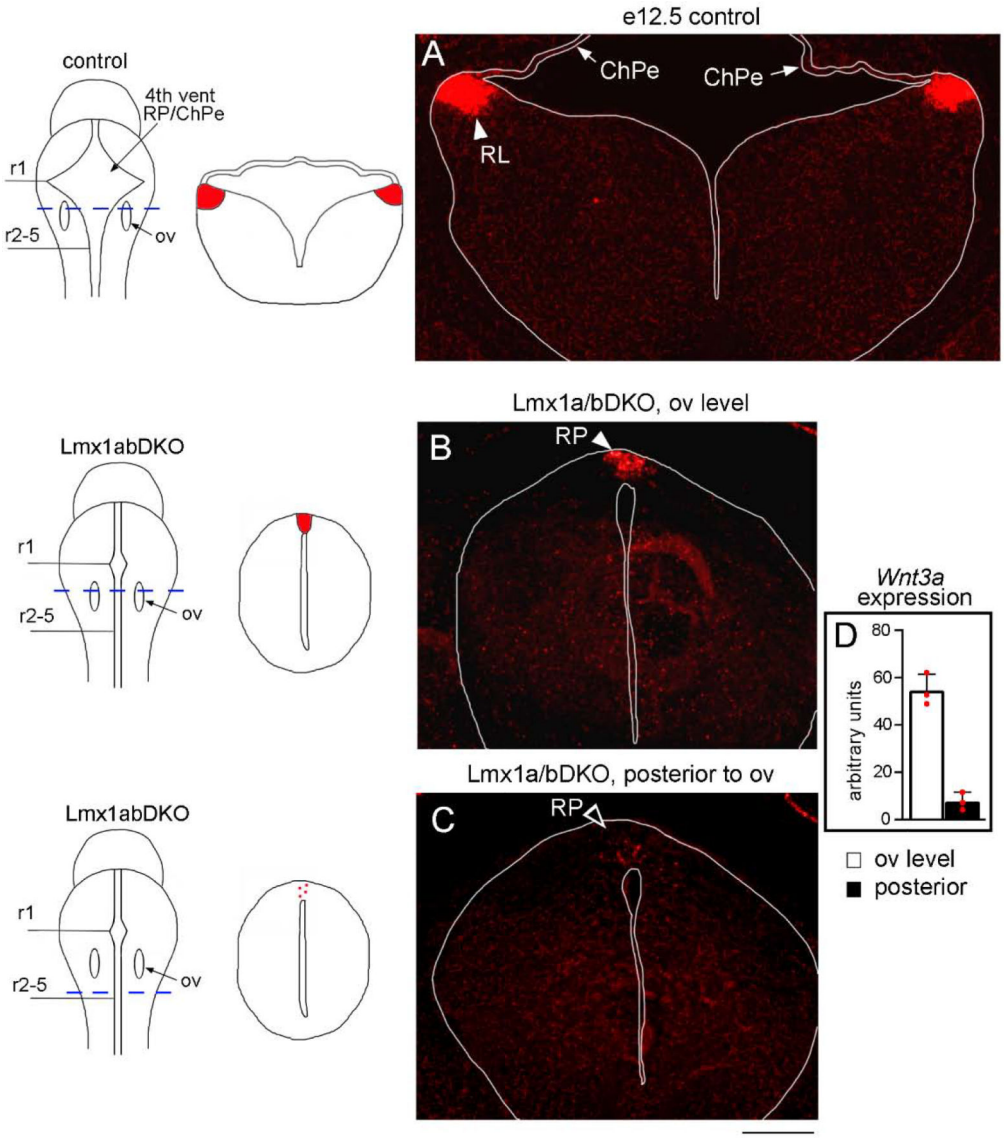

Fig. 8. Ectopic expression of *Wnt3a* in the hindbrain roof plate in *Lmx1a/b* DKO embryos.

Transverse sections of e12.5 hindbrain stained with *Wnt3a* RNAscope *in situ* hybridization. Sections are taken at the level shown by dashed blue line in whole mount brain diagrams. Sections shown in panels A and B are taken at the level of otic vesicles (ov, r4). Section in panel C is posterior to otic vesicles. Tissue morphology on transverse sections is illustrated adjacent to each whole mount diagram. Note, that in contrast to control embryos, in *Lmx1a/b* DKO embryos, the hindbrain does not possess a large ventricle and shows a spinal cord-like morphology. In *Lmx1a/b* DKO embryos, the IVth ventricle roof plate (RP) still occupies the dorsal midline but does not differentiate into the choroid plexus epithelium (ChPe) that covers the IVth ventricle in control embryos (Mishima et al., 2009).

(A) In control embryos, *Wnt3a* is highly expressed in the RL (arrowhead) adjacent to the ChPe but not in the ChPe itself.

(B-D) In *Lmx1a/b* DKO embryos, at the level of otic vesicles, a smaller ectopic *Wnt3a* expression domain was located in the dorsal midline roof plate (RP, arrowhead) (B). At more

posterior levels, *Wnt3a* expression was virtually absent, appearing as just a few dots in the roof plate (open arrowhead) (C). (D) Quantification of RNAscope *in situ* hybridization signal confirmed a significant reduction of *Wnt3a* expression in the posterior hindbrain roof plate relative to the roof plate at the otic vesicles level. n=3 *Lmx1a/b* DKO embryos, *** $p<0.001$.

Scale bar: 200 μm.

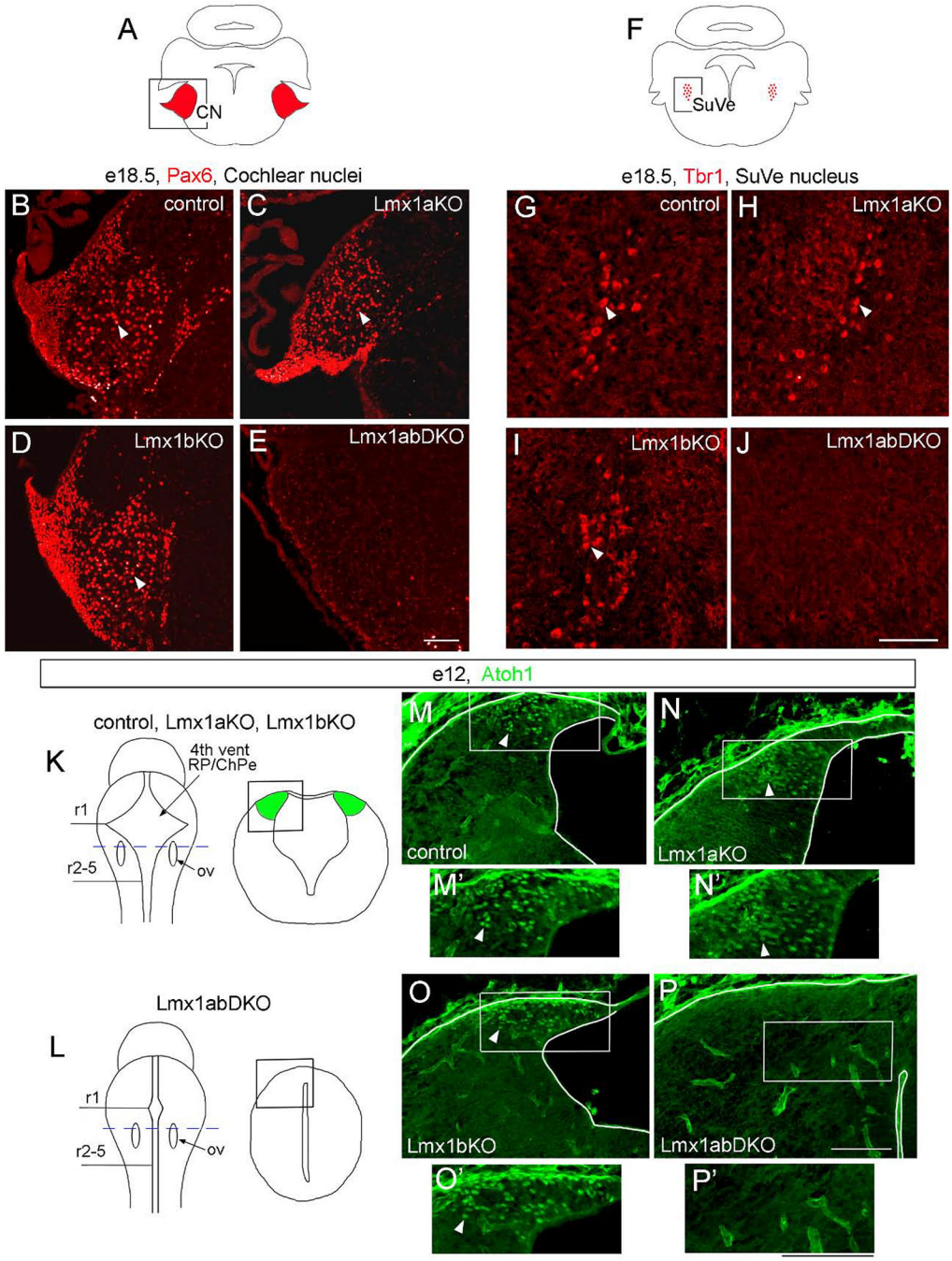

Fig. 9. Simultaneous, but not individual, loss of *Lmx1a* and *Lmx1b* prevents the development of excitatory neurons in cochlear and vestibular nuclei.

Pax6 (B-E), Tbr1 (G-J), and Atoh1 (M-P') immunostained transverse sections of the hindbrain at indicated stages. High magnification panels correspond to regions boxed in adjacent diagrams (A, F, K, L) or low magnification panels.

(A-E) Numerous Pax6+ neurons were present in the cochlear nuclei (CN) of wild type control, *Lmx1a* KO, and *Lmx1b* KO mutants (arrowheads) but were not detected in *Lmx1a/b* DKO embryos.

(F-J) Tbr1+ neurons were present in the superior vestibular nuclei (SuVe) of wild type control, *Lmx1a* KO, and *Lmx1b* KO mutants (arrowheads) but were not detected in *Lmx1a/b* DKO embryos.

(K, L) Diagrams illustrating location of sections showing lower RL in control and *Lmx1a/b* mutant embryos (M-P). Sections were taken at the level of otic vesicles (ov, blue dashed line in whole mount diagrams in K, L). Tissue morphology is illustrated in right diagrams in K and L. (M-P') Numerous Atoh1+ progenitors were present in the lower RL of wild type control, *Lmx1a* KO and *Lmx1b* KO mutants (arrowheads) but not in *Lmx1a/b* DKO embryos.

Scale bar: 100 μm.

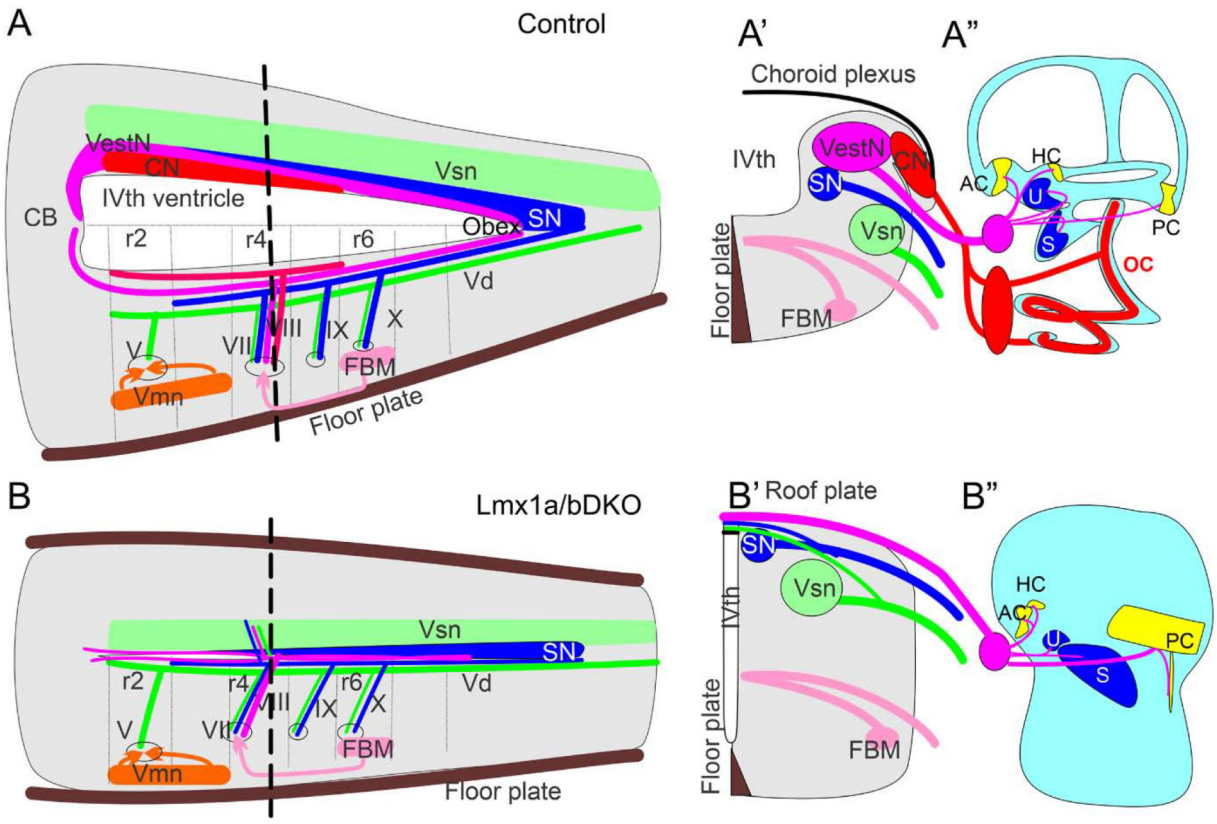

Fig. 10. Simultaneous loss of *Lmx1a* and *Lmx1b* disrupts the inner ear, central projections and cochlear/vestibular brainstem nuclei.

(A, A') Control mice have a large IVth ventricle covered by a choroid plexus. Specific nuclei develop in the alar and basal plate of the hindbrain. CN – cochlear nuclei, which develop in r2–5, VestN – vestibular nuclei, which extend from the caudal cerebellar vermis to the obex, SN – solitary tract nuclei, Vsn – viscerosensory (trigeminal) nuclei, FBM – facial branchial motor neurons, Vmn – ventral motor neurons. Each set of nuclei receives distinct sensory afferents. For example, auditory information is provided by spiral ganglion neuronal projections to cochlear nuclei.

(B, B') In *Lmx1a/b* DKO mice, excitatory neurons of cochlear and vestibular nuclei do not develop. Segregated projections to viscerosensory trigeminal nuclei (Vsn) and solitary tract nuclei (SN) were detected in these mice. Inner ear vestibular afferents project to and cross the roof plate in r4, with limited caudal extension. Similar to inner ear afferents, some solitary tract and trigeminal fibers project to the roof plate. In contrast, basal plate development and innervation (motor neurons) were not significantly affected in *Lmx1a/b* DKO mice.

(A", B") Organ of Corti (OC), spiral ganglion (red oval near the ear in control mice) and spiral ganglion projections were not detected in *Lmx1a/b* DKO mice. In contrast, although altered in size or shape, vestibular inner ear components (AC, HC, U, S, PC and vetibular ganglion - pink circle near the ear) still develop in *Lmx1a/b* DKO embryos.

Table 1.

	OC	AC and HC Innervetion	PC Innervation	Saccule	Utricle	Central auditory projecttions	Central vestibular projecttions
Control	OC	AC + HC	normal	S	U	normal	normal
***Lmxlb* KO**	OC	Partially fused AC +HC	Reduced	S	U	normal	normal
***Lmxla* KO**	OC fused with S, forming CVO	Partially fused AC +HC	Excessive branches	S fused with OC, forming CVO	U	normal	normal
***Lmxla/b* DKO**	none	Partially fused AC +HC	Excessive branches	S	Reduced U	none	Target roof plate, do not extend posteriorly

OC – organ of Corti, CVO – cochlear-vestibular organ, AC- anterior canal crista, HC-horizontal canal crista, PC-posterior canal crista, S-saccule, U-utricle.